Single-molecule quantum-transport phenomena in break junctions

Gehring, Pascal; Thijssen, Jos; van der Zant, Herre

DOI
10.1038/s42254-019-0055-1

Publication date
2019

Document Version
Accepted author manuscript

Published in
Nature Reviews Physics

Nature Reviews Physics **1** (2019)
381 – 396
DOI: 10.1038/s42254-019-0055-1

Single-molecule quantum-transport phenomena in break junctions

Pascal Gehring, Jos M. Thijssen and Herre S.J. van der Zant*
Kavli Institute of Nanoscience, Delft University of Technology, Delft, The Netherlands.
*e-mail: h.s.j.vanderzant@tudelft.nl

Summary
Quantum aspects of transport through single molecules are observable at room temperature. In this Technical Review, we discuss the different processes and energy scales involved in charge transport through single-molecule junctions, the resulting electronic functionalities and the new possibilities for controlling these functionalities for the realization of nanoscale devices.

Key points

- Single-molecule junctions are model systems for the study of quantum mechanical aspects of charge transport at room temperature.
- There are various break-junction techniques for measuring the conductance of single molecules; mechanical break junctions offer excellent statistics, requiring machine-learning analysis techniques, whereas electrical break junctions offer superior gate control for detailed spectroscopy.
- By carefully designing molecular junctions, the energetics can be tuned to enable the construction of molecular diodes or quantum interference devices with conductance changes of several orders of magnitude.
- Sharp resonances in the electrical conductance of a molecule result in high thermoelectric efficiencies, which can be higher than values achieved in bulk materials.
- The electron spin in molecules can be electrically addressed and has applications in switches and qubits.
- The challenge of this interdisciplinary field is to translate quantum-transport phenomena into robust electronic device functionality.

Abstract
Single-molecule junctions — devices in which a single molecule is electrically connected by two electrodes — enable the study of a broad range of quantum-transport phenomena even at room temperature. These quantum features are related to molecular orbital and spin degrees of freedom and are characterized by various energy scales that can be chemically and physically tuned: level spacings, charging energies, tunnel couplings, exchange energies, vibrational energies and Kondo correlation energies. The competition between these different energy scales leads to a rich variety of processes, which researchers are now starting to be able to control and tune experimentally. In this Technical Review, we present the status of the molecular electronics field from this quantum-transport perspective with a focus on recent experimental results obtained using break-junction devices, including scanning probe and mechanically controlled break junctions as well as electromigrated gold and graphene break junctions.

[H1] Introduction

Today's electronic components comprise nanoscale building blocks with varying functionalities that act as conducting interconnects, switches or sensing elements. For almost two decades, researchers in the field of molecular electronics have aimed to condense electronic functionalities into single molecules by chemical design[1,2]. However, before molecular electronic components can be

fabricated, the single-molecule building blocks need to be characterized in junctions to understand their electronic behaviour. To this end, tremendous advances have been reported and reviewed[3,4,5,6,7,8,9]; for example, single-molecule transistors,[10] switches[11] and diodes[12,13,14,15] have been demonstrated. Nevertheless, it is still difficult to experimentally identify the physical mechanisms behind these functionalities or how single molecules arrange in an electronic junction; therefore, predictions based on existing models for molecular device functionality are often unreliable. The realization of functional molecular devices thus requires deeper understanding of the quantum-transport features and experimental elucidation of the intrinsic structure–property relationships of different molecules. In this Technical Review, we assess the recent developments in single-molecule electronics and highlight the fascinating quantum-transport properties using recent results from break-junction experiments as examples. A brief summary of the computational efforts in understanding quantum-transport phenomena using ab initio approaches is provided in the Supplementary Information.

A single-molecule junction consists of a molecule connected to two electrodes — one at either end; sometimes there is a third terminal (known as the gate electrode) that can shift the electrostatic potential of the molecule independently from the potential of the electrodes. Junction fabrication involves breaking a conducting wire, and this can be achieved using one of several techniques (Fig. 1a–c). In a break junction, the conductance along the backbone of the molecule is probed. Thus, we do not consider molecules lying on a surface, for which the current flows in the perpendicular direction; these are typically studied by means of low-temperature scanning tunnelling microscopy.

The nature of the anchoring determines the electronic molecule–electrode tunnel coupling, Γ_i, where i is L or R for the left and right electrode, respectively. The total tunnel coupling is given by $\Gamma = \Gamma_L + \Gamma_R$. Although the electrons in the electrodes have a continuous spectrum of energy states, on the isolated molecule, they occupy a discrete set of levels that, in the junction, are broadened to a width of order Γ. This set of levels gives rise to a rich variety of transport phenomena, the accessibility of which depends on the energy scales of Γ, k_BT (where k_B is Boltzmann's constant and T is the temperature) and the energy cost to add an extra charge to the molecule. This latter contribution is known as the addition energy, $E_{add} = 2E_C + \delta$, where the charging energy $E_C = e^2/2C$; here, C is the total junction capacitance, δ is the quantum level spacing (that is, the orbital contribution) and e is the elementary charge. If Γ is smaller than both k_BT and E_{add}, Coulomb blockade and incoherent transport through two-step single-electron tunnelling prevails — this is the weak coupling regime. In the opposite, strong coupling regime, coherent transport is typically observed, usually involving off-resonant transport, although for very small molecules, such as H_2, resonant transport applies, resulting in conductance values close to the conductance quantum[16].

A unique aspect of molecular junctions is the interplay between the different energy scales that determine the transport characteristics. These energy scales are the electronic coupling (~0.1–1 meV), the temperature (which varies from 2 μeV to 25 meV) and the addition energy (often >100 meV). The vibrational and spin degrees of freedom are of special interest, as these features are specific to molecular transport and are not easily accessible in transport experiments with other systems, such as inorganic quantum dots. For vibrational modes (Box 1), the relevant parameters are the mode energy ($\hbar\omega$ = 1–300 meV, where $\hbar$ is the reduced Planck's constant and ω is the angular frequency) and the electron–phonon coupling strength. The latter parameter determines the extent to which electron flow is affected by the presence of phonons. As single molecules are floppy systems, this coupling can be much stronger than in, for example, crystals and leads to novel transport phenomena such as the Franck–Condon blockade of transport (Box 1).

Chemical design offers various ways to incorporate spin degrees of freedom into a molecule. The coupling between spin and transport forms an interesting field of research called molecular

spintronics. Upon the introduction of spin degrees of freedom, additional energy scales must be considered, such as the exchange energy between interacting spins, *J*. Spin-dependent correlations between the electrons on the molecules and the conduction electrons in the electrodes can give rise to a so-called Kondo peak in the transmission at zero bias; this peak is quantified by a Kondo temperature, T_K, above which the anomaly disappears. In practice, experimental exchange energies and the Kondo temperature vary between a few tenths of a meV to several meV. If the molecule exhibits magnetic anisotropy (that is, if the spin has a preferred orientation along an easy axis and therefore acts as a miniature magnet), the axial anisotropy parameter, *D*, may become relevant. This parameter can be viewed as a measure for the extent to which the preferred orientation is maintained, and the transverse anisotropy parameter, *E*, is responsible for quantum tunnelling of the spin orientation between its up and down state. *D* is the largest energy scale of the two with values <<1 meV, and *E* is typically in the μeV range. The electrodes can also be made of a superconducting material, in which case the superconducting gap, Δ, becomes relevant.

Although there are different energy scales associated with the different break-junction platforms (Fig. 1a–c) and transport mechanisms (Fig. 1d), it is important to note that there are no sharp boundaries between the different regimes. The different single-molecule junctions have distinctive properties, which are summarized in Table 1. We begin by describing the break-junction platforms used to perform single-molecule conductance measurements before discussing different aspects of quantum-transport phenomena, including the single-level model, orbital engineering beyond the single-level model, quantum interference effects, quantum thermopower and heat transport as well as single-molecule spintronics. We conclude by discussing future research directions.

[H1] Single-molecule break junctions

There are two main break-junction techniques: mechanical and electrical break junctions. Mechanical break junctions (Fig. 1a,b) are realized by means of scanning tunnelling microscopy (STM) to form a STM break junction (STM-BJ)[17,18] or with nanolithography techniques to form mechanically controlled break junctions (MCBJs)[19,20]. In the STM-BJ approach, a metallic tip is usually gently pushed onto a metallic substrate on which the molecules are deposited. Upon retracting the tip from the substrate, atomically sharp contacts can form, and the conductance (*G*) of a molecule trapped between the substrate and tip is measured as a function of distance (*d*), resulting in a conductance-breaking trace. The junction lifetime is limited by the drift in the position of the tip. The STM-BJ technique is not to be confused with scanning a substrate, typically at low temperature with a defined sample-to-tip distance, to image molecules lying on the surface and perform spectroscopy on them.

Breaking traces are also measured in a MCBJ experiment, although the contact geometry is different: in this case, bending of the device breaks a conducting wire, which yields an atomically sharp contact pair. Just like in STM-BJs, current–voltage (*I*–*V*) characteristics and conductance-breaking traces can be measured; however, the MCBJ approach enables a more systematic study thereof as junction lifetimes are much longer owing to superior mechanical stability (Table 1). Especially at low temperatures, the MCBJ set-up is often used to record *I*–*V* characteristics and to perform inelastic-tunnelling spectroscopy of vibrational modes. Both mechanical break-junction methods can be used to measure the conductance as a function of time at a fixed distance (sometimes called a blinking experiment). In such an experiment, a sudden increase in the conductance signals the trapping of a molecule between the two electrodes, but additional information about the junction configuration is difficult to obtain. Thus, one has to be cautious in interpreting the data as changes in the contact configuration may obscure the interpretation.

Advantages of the STM-BJ technique are its simplicity and the larger dimensions of the source and drain electrodes. The larger dimensions enable[21], for example, the simultaneous measurement of the conductance and force between the two electrodes as well as the incorporation of an

electrochemical gate[22] while the scanning tunnelling microscope tip is covered by an insulating layer. Gating in a MCBJ has been demonstrated with an aluminium gate electrode[23]. The magnitude of gate-induced level shifts varies for the different devices (Table 1), with the electrochemical STM-BJ (that is, a STM-BJ placed within an electrochemical cell) achieving the largest electrochemical level shifts. Although the liquid environment of the electrochemical cell imposes restrictions, working in solvents enables the electronic response of molecular junctions to the addition of chemicals to be probed in situ. Methods have therefore been developed to fabricate MCBJ junctions that can be used to study molecular transport in a solvent by coating the metal electrode with a thin insulating oxide layer[24,25]. In this respect, graphene is an promising electrode option, and the first graphene-based MCBJs have been fabricated[26,27].

Electrical break junctions (Fig. 1c) are formed by electromigration[28], a process in which a voltage is ramped across a metallic wire with a small cross section until it breaks, resulting in the formation of a nanometre-sized gap between two electrodes. Feedback control[29] and self-breaking schemes[30] have been developed to gain control over this gap size. An advantage of this technique is that the junctions can be fabricated directly on a gate dielectric, enabling strong gate coupling. However, compared with mechanical break junctions, acquiring statistical information about electrical break junctions is much harder. Using this approach, the formation yield of molecular junctions is typically low (10%), and because every junction requires a new device to be made, the study of a large number of molecular junctions is time consuming. Furthermore, gold electromigrated junctions are not stable at room temperature owing to the migration of gold atoms along the electrode surfaces at temperatures above ~200 K. Graphene is an alternative electrode material that does not suffer from this instability, and (few-layer) nanometre-separated graphene electrodes are made in a process similar to that used for gold electromigration. The fabrication technique is often termed electroburning as excess carbon atoms are removed in a reaction with oxygen[31,32,33] or by sublimation under vacuum[34]. These junctions with graphene electrodes are stable at room temperature, although the formation of spurious graphitic islands necessitates control experiments involving gate-dependent measurements, preferably at low temperatures[35,36].

Various anchoring strategies have been used to attach molecules to metallic electrodes[37,38], although details on the exact contact geometries involved and how they influence transport are still being discovered. Strategies can be divided into those based on physisorption or chemisorption. For gold electrodes, thiol anchoring is often used to achieve a strong mechanical, chemisorbed molecule–electrode connection. Different anchoring positions are possible as the sulfur atoms can bind to gold surfaces at adatoms, step edges or hollow sites, each of which exhibits a different mechanical and electronic coupling strength (and thus conductance). Other end groups for chemisorption to gold include amine, carboxyl, cyano and pyridine groups or direct gold–carbon binding using different protocols. Charge transfer across the molecule–electrode interface can lower the orbital levels, favouring transport via the lowest unoccupied molecular orbital (LUMO) (for example, when using pyridine or cyano groups), whereas thiol end groups connected to gold tend to raise the orbital levels, favouring transport mediated by the highest occupied molecular orbital (HOMO). An example of a physisorbed contact is through-space tunnelling from the electrode to, for example, the π clouds of benzene rings, which may then form an alternative, coexisting route for charge injection. For physisorbed systems, charge transfer does not have an important role. For graphene electrodes, both physisorption attachment strategies (through π–π stacking) and chemisorption strategies based on amide bond formation with carboxyl groups at the graphene edges are used.

To unveil effects associated with small energy scales in a molecule, the best option is an electrical break junction owing to the weak coupling, which keeps the linewidth of molecular levels small. A further advantage of this technique is gate control, which enables detailed low-temperature spectroscopy of magnetic, electronic or vibrational excitations and redox states. However, if generic features of a molecule, rather than those of an individual specimen, are of interest, mechanical break

junctions are the platform of choice. Mechanical break junctions are generally used to study the structure–property relationships of a series of molecules. The statistical approach of probing different junction configurations and molecular conformations, the possibility of studying the interactions with solvents and combining conductance experiments with, for example, simultaneous measurements of the force holding the molecular junction together, make this a versatile technique for room-temperature studies. In terms of scalability, one should opt for the planar, on-chip fabrication break-junction methods, of which wafer-scale fabricated crack-defined break junctions are an interesting recent example[39].

[H1] Single-level model

When discussing transport through single molecules, it is necessary to distinguish between coherent and incoherent, resonant and off-resonant, and elastic and inelastic transport. Typically, mechanical break junctions probe off-resonant, coherent transport with a distance dependence that is characterized by the β-decay parameter; a smaller β corresponds to more efficient transport. The conductance in this regime is independent of temperature as long as the molecular orbital levels are sufficiently far away from the Fermi level of the electrodes. This approach works well for small molecules (with lengths of 1–3 nm) and relatively large electronic couplings, but as the molecular length increases or the coupling strength decreases, there is a crossover to the incoherent, hopping regime. Transport in the incoherent, hopping regime is temperature dependent, and, in the case of hopping across multiple sites, the conductance increases with a power-law dependence on molecular length instead of the stronger exponential dependence in the coherent regime. We discuss below the coherent, off-resonant transport regime, two-step hopping and the crossover between the two regimes.

[H2] Current–voltage characteristics. If the electronic coupling is smaller than the molecular-level separation, transport is usually dominated by individual molecular orbitals. In this regime, the single-level model gives insight into the transport features and is therefore frequently used to interpret experimental data. To appreciate this approximation, chemical potential diagrams (Fig. 2a) are useful. In a chemical potential diagram, the left and right electrodes are depicted as Fermi functions with filled states up to the Fermi energy (ε_F); the rounding off at the Fermi energy indicates finite temperature. The energy states of the molecule are shown as a series of levels broadened owing to hybridization with the metallic electrodes, to which the molecule is coupled via tunnel barriers. The orange line in this figure represents the energy-dependent transmission function, $T(\varepsilon)$, of these broadened levels. Note that in a non-interacting system, the single- particle energies are identical to the chemical potentials, in which case, these terms can be used interchangeably. $T(\varepsilon)$ thus represents the probability for an electron injected at energy ε at one end of the molecule to be transported to the other end. The levels can deviate from those in the gas phase as image charge effects and (partial) charge transfer shift them[40].

Knowing $T(\varepsilon)$, the current, which is a measure of how many charges are transmitted through the molecule per unit time, can be calculated using the Landauer formula. If the electron–electron interactions are neglected, the current is given by

$$I = \frac{e}{h}\int T(\varepsilon)[f_{\mathrm{L}}(\varepsilon) - f_{\mathrm{R}}(\varepsilon)]\mathrm{d}\varepsilon \qquad (1)$$

where h is Planck's constant and $f_{\mathrm{L}}(\varepsilon)$ and $f_{\mathrm{R}}(\varepsilon)$ are the Fermi distributions in the left and right electrode, respectively. As a first approximation to describe measured *I*–*V* curves, only the level closest to the Fermi energy of the leads at an energy ε_0 and with a lifetime broadening Γ is considered (Fig. 2b). In this single-level model, using equation 1, the current at low temperatures can be calculated analytically when the electrode couplings Γ_{L} and Γ_{R} are assumed to be energy independent (the so-called wide-band limit). The current varies stepwise with bias[41,42]:

$$I = 4\frac{G_0}{e}\frac{\Gamma_{\mathrm{L}}\Gamma_{\mathrm{R}}}{\Gamma_{\mathrm{L}}+\Gamma_{\mathrm{R}}}\left[\arctan\left(\frac{\varepsilon_0+(1-\alpha)eV}{\Gamma_{\mathrm{L}}+\Gamma_{\mathrm{R}}}\right) - \arctan\left(\frac{\varepsilon_0-\alpha eV}{\Gamma_{\mathrm{L}}+\Gamma_{\mathrm{R}}}\right)\right] \qquad (2)$$

Here, the fit parameters are ε_0, Γ_L and Γ_R and the asymmetry parameter $\alpha = C_R/(C_L + C_R)$, where C_L and C_R are the capacitive couplings to the leads; and G_0 is the conductance quantum, defined as $2e^2/h$. In the presence of a gate, the gate voltage needs to be added to ε_0 after multiplication by a `gate coupling factor', and the bias voltage division has to be modified as described in ref.[43].

The *I*–*V* curves calculated using equation 2 are strongly dependent on the parameters (Fig. 2c–f). The *I*–*V* curves have an S-like shape with a steep current increase when the electrochemical potentials of the electrodes approach the resonant condition with the level at ε_0 (Fig. 2c). For bias voltages exceeding $eV = 2\varepsilon_0$, the current saturates at

$$I_{\mathrm{sat}} = 4\frac{G_0}{e}\frac{\Gamma_L\Gamma_R}{\Gamma_L+\Gamma_R} \qquad (3)$$

Changing the total tunnel coupling or the ratio of the tunnel couplings (Γ_L/Γ_R) result in a change in this saturation current (Fig. 2d,e). Note that the *I*–*V* curve remains symmetric in the latter case. Asymmetric, rectifying-like *I*–*V* characteristics appear when the capacitive couplings, entering as the asymmetry factor, to the two electrodes are no longer equal (Fig. 2f). In the literature, the ratio of the tunnel couplings is often used as an estimate for the asymmetry in the voltage drop instead of the capacitive coupling. It is, however, useful to distinguish these essentially different couplings: the tunnel coupling depends exponentially on the barrier thickness, whereas the capacitances scale with the inverse of the barrier thickness for large molecule–electrode separations. For small separations, the capacitive interaction may exhibit a peak beyond which it decreases with decreasing separation[44]. Finally, we stress that the situation in a real molecule is more complex than that in the single-level model, and self-consistent quantum chemistry calculations are necessary[45] to capture the contributions of the other levels and the precise shape of $T(\varepsilon)$ for the each of the levels involved.

[H2] Level alignment. The single-level model is frequently used to fit *I*–*V* data in the strongly coupled regime to quantify the level position and broadening. Although the curve shape at low bias (far away from resonance) is typically well described, the values of the fit parameters (ε_0 and Γ) have to be interpreted with more care: as ε_0 is extracted from a low-bias *I*–*V* curve, it gives only an estimate for the real level position. To verify the level position, high bias voltages would need to be applied to reach the resonant transport condition. However, it is difficult to reach this condition; bond breaking[46], Coulomb interactions or instabilities associated with vibrational heating[47] or charging of the molecule have been proposed as explanations for this difficulty.

One approach to gain additional information about the level alignment is the use[48] of transition voltage spectroscopy, which can potentially reveal the molecular levels through a common procedure applied to Fowler–Nordheim tunnelling. By plotting the measured *I*–*V* curve as $\ln(I/V^2)$ versus $1/V$, a dip appears, the position of which is related to the level position. The appealing feature of this procedure is that the molecular junctions do not have to be in the resonant condition. However, an *I*–*V* curve of an empty junction yields a similar dip, which may be wrongly interpreted as a molecular junction with a particular level alignment. In addition, the voltage profile along the molecular junction influences the determination of ε_0. It is thus necessary to be careful when applying transition voltage spectroscopy to experimental data; at most, qualitative information can be obtained[49]. Consequently, other methods that can reveal information about the level alignment are being proposed, such as one based on a Taylor expansion of the *I*–*V* curve, with the goal to discriminate between different transport mechanisms[50]. An alternative, direct approach to gain insight into the ε_0 and Γ values is to measure $T(\varepsilon)$ directly by using a gate voltage to shift ε_0 and simultaneously record the low-bias conductance. For this approach, an efficient gate is needed to span a large energy window in $T(\varepsilon)$. An example is liquid gating in STM-BJs, which has been used to map out $T(\varepsilon)$ for an energy range of >1.5 eV (ref. [51]).

[H2] Incoherent transport. For small Γ, the electron dwell time on the molecule suffices to dephase the quantum state and gives rise to incoherent transport. For small molecules with one main (redox) site, transport evolves into a two-step hopping process, and the analytical expression of equation 1 can no longer be used to describe the *I*–*V* curves. In this regime, the *I*–*V* curves display a gap around zero bias with a very low conductance; the step-like increase in current when the level is pushed into resonance is still present. There are many examples of such *I*–*V* curves in the literature. As these junctions are typically made using electromigration, the gate voltage can be used to achieve the resonant condition and to reproducibly charge the molecule with an additional electron or hole. The crossover between the weakly and strongly coupled regimes remains to be studied in detail, and only a few experiments have been performed to probe this intermediate regime. In MCBJs[52] at low temperatures, a stretching-induced transition from the strong to the weak electronic coupling regime has been observed, involving a large renormalization of ε_0 and Γ. Furthermore, current blockade has been reported at room temperature in a STM-BJ study on a cobalt chalcogenide cluster[53]. Other developments include investigations of the inverted Marcus regime[54] in transport as well as considerations of the importance of nuclear tunnelling even at elevated temperatures[55].

[H1] The two-level model

The single-level model treats the molecular junction as a 'molecular wire' characterized by a conductance determined by ε_0 and Γ. No additional electronic functionality, such as rectification, can be expected from such a model. To achieve additional functionality, it is necessary to go beyond the single-level model and, for example, consider two molecular moieties in series that are weakly coupled to each other by a small tunnel coupling, τ (Fig. 3a top, right panel). The coupled moieties form two levels with an energy separation of 2τ. The key difference from the single-level model is that there is a substantial drop in the applied bias voltage within the molecule, that is, across the barrier between the two levels. Consequently, when the bias is increased, the two levels are pulled apart owing to capacitive effects, to the extent that at some point they are no longer resonant. The current then decreases with increasing bias voltage, resulting in a negative differential conductance.

Realization of this two-level model[56] has been demonstrated with a molecule consisting of two conjugated groups connected by a non-conjugated core, which provides the internal barrier. This structure yields a HOMO and HOMO – 1 separated by 2τ with antibonding and bonding character, respectively (Fig. 3a left, bottom panel). The HOMO and HOMO – 1 orbitals can now be transformed into a set of equivalent localized molecular orbitals (LMOs) through addition or subtraction, yielding a LMO on the left part of the molecule (L-LMO) and one on the right part of the molecule (R-LMO). This transformation converts the energy-basis representation of the two-level model into an equivalent site-basis representation, which is more intuitive when explaining transport through this molecule under the influence of a bias. Analytical results for the two-site model show excellent agreement with the experimental *I*–*V* characteristics (Fig. 3b). By breaking conjugation in the centre of a molecule, a resonant single-molecule tunnel device exhibiting negative differential resistance is thus formed, in which the functionality is embodied in its molecular core.

A further application of the two-level model is to introduce an asymmetry in the level positions such that the two levels are no longer at the same energy at zero bias. This configuration allows for the realization of a diode with very high rectification ratios[57]. As the two levels are not aligned, the system is off-resonant at zero bias and the current is low. When a bias is applied in one direction, the levels are pulled further apart, thereby further reducing the current. However, for the opposite bias polarity, the two levels move towards each other until they are resonant, leading to a high current. This concept was realized experimentally in an asymmetric molecule consisting of two similar conjugated halves connected by a non-conjugated bridge. The asymmetry was introduced by adding electron-withdrawing fluorine groups to one conjugated half, lowering the energy of its orbitals.

MCBJ experiments[58] confirm the expected behaviour: for one bias polarity the current shows a resonant-like peak, whereas for the opposite bias, the current remains low (Fig. 3c).

[H1] Quantum interference

Quantum interference (QI) describes the interference of wavefunctions of quantum mechanical objects, such as particles, photons or electrons. Theoretically, single molecules are ideal hosts for interference effects as their molecular structure can be used to guide electrons through different paths to control QI. These interference effects provide ways of tuning the $T(\varepsilon)$ of molecular junctions, allowing for the design of molecular switches and enabling highly efficient thermoelectrics (see below).

The quantum mechanical wavefunction that describes an electron is complex-valued, that is, it has amplitude and a phase. Thus, whenever multiple transport pathways through a molecule contribute to electrical transport, QI can occur; constructive QI increases the tunnelling probability through the molecule whereas destructive QI blocks electrical transport (Fig. 4a). A notable example of a molecule that hosts QI is a single benzene ring. For molecules in which there is a central benzene ring with para connectivity, there is a phase difference of 2π for charge passing through the HOMO and LUMO orbitals (Fig. 4b). Thus, if both orbitals contribute to transport simultaneously, that is, if the Fermi energy is located between the HOMO and LUMO, constructive interference and consequently enhanced conductance is observed. By contrast, if the central benzene ring has meta connectivity, the HOMO and LUMO orbitals contribute with a phase difference that, for a particular injection energy, can reach π, and therefore destructive QI occurs with a sharp dip in $T(\varepsilon)$ (Fig. 4c,d). The sharpness of this dip, which is caused by the π system, is in practice attenuated by the conductance through the σ bonds. Extending the length of the molecule suppresses the σ-bond conductance.

Direct experimental evidence for this type of QI has been gained from measurements on, for example, benzene rings[59] and oligo(phenylene vinylene) derivatives[60] (Fig. 4b,c). If the central benzene ring has para connectivity to the electrodes, the measured conductance is more than one order of magnitude higher than the conductance in the analogue with meta connectivity irrespective of the connectivity to the anchors[61]. These connectivity rules have been generalized for polycyclic aromatic hydrocarbons: the connectivity of a polycyclic aromatic hydrocarbon to the electrodes dictates whether constructive or destructive QI effects occur in the core and thus determines the resulting conductance. In the regime in which electron–electron interactions can be neglected, this effect can be quantified using magic ratios: the conductance of the same molecule connected to the electrodes at different points *i*–*i*′ and *j*–*j*′ is given by the ratio of two integers $(M_{ii'}/M_{jj'})^2$, which have been calculated for different molecules[62].

Another type of QI results from the interference between a delocalized backbone state and a localized state that couples to the delocalized state but not to the electrodes (sometimes called a stub-structure). Depending on the levels on the backbone and the side group (Fig. 4e), destructive interference may suppress the conductance. The resulting $T(\varepsilon)$ possesses asymmetric features (Fig. 4f), which have been proposed to be generic for the transmission of cross-conjugated molecules[63]. Interference is a very common phenomenon in optics, wherein a light beam from a collimated source can be split and directed along different optical pathways. The interference between the beams contains information about their phase difference, which may have been acquired on their way. A QI effect analogous to this 'Mach–Zehnder interferometer' in optics can be observed in single molecules with multiple parallel transport paths. For example, this QI effect is evident upon comparing the conductance of a molecule with a single-channel CH_2–benzene–CH_2 backbone and a molecule with two parallel CH_2–benzene–CH_2 backbones and thus parallel transport pathways[64]. The conductance of the molecule with the parallel backbones was approximately three times that of the single-channel molecule and is larger than the value of two classical, parallel channels obtained by Kirchhoff's law.

This increased conductance can be attributed to constructive QI. Besides QI in delocalized π systems, QI in σ systems of saturated silicon-based molecules was recently reported[65].

Control of destructive QI through chemical gating has been demonstrated in *meta*-oligo(phenylene ethynylene) derivatives by substituting a nitrogen atom into the central benzene ring[66] . Owing to cross-conjugation, anthraquinone has a low conductance; however, its oxidation state can be altered using an electrical[67] or electrochemical[68] gate. By adding an extra electron, cross-conjugated anthraquinone becomes a linearly conjugated dihydroxyanthracene and destructive interference is switched off, leading to an enhancement of the conductance by more than one order of magnitude (Fig. 4g). Electrochemical gating has recently also been employed to map $T(\varepsilon)$ of molecules with decreased conductance due to destructive interference.[69,70] Another way of QI tuning is the mechanical manipulation of π–π stacking[71]. Furthermore, by stretching or compressing a single oligo(phenylene ethynylene)-linked [2.2]paracyclophane molecule, mechanical gating[72] was used to push the interference dip through the Fermi energy, providing direct proof of the existence of interference in a single molecule.

[H1] Quantum thermopower and heat transport

Thermoelectric effects, which manifest from the interplay between heat and charge currents, have gained increasing attention in the field of molecular electronics over the past 10 years. These effects offer an alternative way of mapping the $T(\varepsilon)$ of a molecular junction (see below). The advantage is that measurements are recorded under zero-bias conditions; thus, the molecular junction is not disturbed by the bias electric field. Moreover, single molecules are predicted to be excellent heat-to-electricity converters. The efficiency of thermoelectrics is given by the dimensionless figure of merit, $ZT = (\sigma S^2/\kappa)T$, where σ and κ are the electrical and thermal conductivities, respectively, and $S = V_{th}/\Delta T$ is the Seebeck coefficient (often called thermopower), which quantifies the electromotive force (V_{th}) created by a certain temperature bias (ΔT). Note that κ contains contributions from both electrons (κ_{el}) and phonons (κ_{ph}), and both have to be minimized in order to increase ZT. In bulk thermoelectrics, progress in increasing ZT is hampered by the fact that the parameters S, σ and κ_{el} cannot be optimized independently: a high Seebeck coefficient is accompanied by low σ, and high σ by high κ_{el}. It will be interesting to investigate if this unfavourable coupling between these quantities can be circumvented in single molecules by exploiting QI effects in the electron and phonon channels separately with the aim to minimize κ_{el} and κ_{ph} while increasing σS^2 (ref. [73]).

As discussed above, the current through single-molecule junctions can be estimated using the Landauer approach. Let us assume a situation in which one electrode is at a higher temperature than the other (Fig. 5a). The Fermi–Dirac distribution of the hot electrode broadens more than that of the cold electrode, and, consequently, the occupation of higher-energy states in the hot electrode increases the tunnelling probability through the single level. The resulting thermal tunnelling current, I_{th}, is proportional to the temperature difference, $\Delta T = T_L - T_R$ (where T_L and T_R are the temperatures of the left and right electrodes, respectively), with $I_{th} = -GS\Delta T$. Under open-circuit conditions, the voltage drop is $V_{th} = -S\Delta T$. Assuming that $T(\varepsilon)$ varies slowly on the energy scale of k_BT and that $k_BT \ll \varepsilon_F$, the Sommerfeld expansion of equation 1 yields

$$S = \frac{-\pi}{3}\frac{{k_B}^2 T}{e}\frac{1}{T(\varepsilon_F)}\frac{\mathrm{d}T(\varepsilon)}{\mathrm{d}\varepsilon}\bigg|_{\varepsilon_F} \qquad (4)$$

Equation 4 gives an intuitive feeling for the information contained in the Seebeck coefficient; the last term in this equation is a measure for the electron–hole asymmetry at the equilibrium Fermi energy. A large Seebeck coefficient is achieved when this asymmetry is large, which will be the case if the transmission probability possesses sharp transmission features close to the Fermi energy (Fig. 5b).

Sharp transmission features can arise by reducing the tunnel coupling or by introducing QI effects[74,75,76], albeit at the expense of reducing the conductance and thus the output power. Furthermore, as the sign of the Seebeck coefficient is given by the sign of the slope of $T(\varepsilon)$ at the Fermi energy, it can also be used to determine if transport is dominated by the HOMO or the LUMO[77]. Note that the Seebeck coefficient is independent of the number of molecules probed in parallel; however, it is additive for molecules in series.

The thermoelectric properties of numerous different single molecules have been measured using STM-BJs, in which a temperature difference ΔT can be obtained by either heating the scanning tunnelling microscope tip or the substrate[78]. The Seebeck coefficient has been extracted from thermocurrent[79] and thermovoltage[80] measurements. Thermoelectric single-molecule measurements have also been performed using MCBJs[81]. The break-junction experiments have verified[82] the correlation between level alignment, the sharpness of transmission features at the Fermi energy and the sign and magnitude of the Seebeck coefficient, as predicted by equation 4 (ref.[83]). Additionally, electron-donating or electron-withdrawing side groups[84,85] or anchoring groups[86] can shift the HOMO or LUMO level position (or an interference dip) with respect to the Fermi energy, which results in a change in the Seebeck coefficient. The Seebeck coefficient can also be varied by using metal contacts with different work functions[87]. Furthermore, the sign and magnitude of the Seebeck coefficient can be controlled mechanically by pressing molecules with the tip of a scanning tunnelling microscope[88] (Fig. 5c). The level alignment can be changed using an electrical gate, an approach that has been demonstrated in gold-based[89] and graphene-based[90] electromigrated junctions. In the latter, a reversal of the sign of the Seebeck coefficient was achieved (Fig. 5d).

A current hot topic is the study of thermal transport effects (that is, thermal conductivity) or the interplay between electrical transport and heat transport (that is, the Peltier effect and Joule heating) in single-molecule junctions. To this end, ultrasensitive thermometry has been implemented into STM-BJs by thermally coupling a resistance thermometer or a thermocouple to the scanning tunnelling microscope tip. This set-up enables the measurement of the heat dissipation of single molecules owing to Joule heating[91] or the conversion of charge current to heat current owing to the Peltier effect[92]. Over the past couple of years, improvements in STM-based nanoscale calometry have enabled the study of heat transport through single gold atoms[93,94]. The same devices could be readily used for measuring the thermal conduction in single-molecule junctions. Alternatively, the thermal transport behaviour of single molecules can be characterized in their electrical noise spectra under thermal biasing. By measuring the electrical noise of H_2 molecules and single gold atoms in MCBJs under thermal bias, a new form of electrical noise, termed ΔT noise was observed[95]. This noise, which is a result of quantized heat transport, scales with the square of the temperature difference across the junction. Thus, this noise could enable the estimation of the temperature drop across molecular junctions without the need of sophisticated calometry.

[H1] Single-molecule spintronics

In spin-based electronics or, in short, spintronics, the electron spin is used as the carrier of information instead of its charge. Spintronics traditionally involve the use of semiconductors or metals. However, the (magnetic) properties of molecules are more versatile than those of purely inorganic materials, opening doors for applications in, for example, quantum technologies[96]. Here, we concentrate on molecular spintronics at the single-molecule level, which is the ultimate step in downscaling spin-based devices.

When electronic spin degrees of freedom are relevant to transport, the spin selection rules need to be considered. The total spin can change only by ±1/2 in the single-electron tunnelling regime and by 0, ±1 in the co-tunneling regime, in which, one electron leaves the molecule and is replaced by another electron in a single process. For high-spin molecules, similar rules exist for the *z* component

of the spin. Transport properties connected to spin degrees of freedom typically manifest as subtle features, such as the appearance of (low-energy) magnetic excitations connected to (anti-)ferromagnetic exchange couplings (Fig. 6a) and Kondo physics with a characteristic conductance peak at zero bias (Fig. 6b). In the case of high-spin molecules, additional features may arise as a result of magnetic anisotropy in single-molecule magnets[97], low-spin–high-spin switching in spin-crossover compounds[98,99,100], unexpectedly high magnetoresistance effects[101] or spin blockade, leading to current suppression[102] (Fig. 6c). Single-molecule magnets form an interesting family of molecules as their anisotropy can lead to non-linear spectroscopic features with respect to the applied magnetic field[103] (Fig. 6d) or to applications in qubit spin transistors[104,105,106].

The Kondo effect deserves special attention as it has been studied in a wide variety of molecular compounds. This effect manifests as a zero-bias anomaly in transport and is observed for molecules with an odd charge occupation, that is, for molecules with a net spin (Fig. 6b). The first reports of this effect date back to early electromigrated molecular transistors[107,108]. Subsequent work focused on mechanical manipulation[109] of the Kondo correlations[110] and the interactions with vibrational degrees of freedom[111]. Usually, spins in molecules are introduced with the presence of metal ions; all-organic radicals, however, are also magnetic molecules as their partially filled orbitals possess a net spin and they have been shown to behave as prototype spin-1/2 systems[112,113]. An advantage of using organic molecules is that the Kondo energy scale is well separated from the charging energy and quantum level spacing, $k_B T_K << E_C$ and $k_B T_K << \delta$, enabling a detailed comparison with theoretical calculations. Not only is the Kondo effect used as a spectroscopic tool to identify the presence of a net spin on the molecule, it also enables the study of new phenomena involving many-body charge states. In molecular transistors, these phenomena include the observation of the underscreened Kondo effect[114,115] and singlet–triplet quantum phase transitions[116]. Further details on the (exotic) Kondo physics in molecular junctions can be found elsewhere[117,118].

A prototype spintronics application is a spin valve, a device that changes its resistance when the relative orientation of the magnetization in the electrodes changes. To realize such a spin-valve-based molecular junction, ferromagnetic electrodes can be used to contact the molecule, with one electrode for spin-polarized current injection and one acting as a spin detector. However, contacting individual molecules in combination with using the ferromagnetic materials needed for spin injection and/or detection remains challenging. Oxidation of the ferromagnetic material is one of the complications as the resulting oxide barriers may substantially lower current levels. Another issue is the reliability of the anchoring of the molecules to ferromagnetic materials.

Although experiments with MCBJs have been reported[119,120,121], the first experiments with ferromagnetic electrodes were performed with electromigrated break junctions using C_{60} as a reference molecule. Since the first study in 2004 (ref.[122]), subsequent studies have emphasized the importance of hybridization of the ferromagnetic substrate states with the C_{60} molecular orbitals to explain the large negative tunnelling magnetoresistance[123], the precise electrode–molecule geometry and the associated coupling asymmetry[124]. In explaining the electrochemical gate response, measurements on a bipyridine derivative also highlighted the importance of the molecule–ferromagnetic electrode interface[125]. An intriguing possibility is the observation of spin filtering by chiral, nonmagnetic molecules without the need of spin injection[126]; spin-polarized currents can thus be realized without the use of an applied magnetic field. Spin-state detection still requires the use of a ferromagnetic tip, as has been reported in a STM-BJ[127].

An emerging topic within the field of molecular spintronics is the interplay of molecular spins with superconductivity. Superconducting contacts connected to magnetic spins on a molecule may exhibit intriguing phenomena associated with the competition between Cooper pairing and Kondo screening, which breaks the Cooper pairing and leads to the formation of sub-gap excitations called Shiba states[128]. The first experimental study[129] was on C_{60}-based transistors with electromigrated

aluminium electrodes that displayed the coexistence of Coulomb repulsion, Kondo physics and superconductivity over a broad range of electronic coupling strengths. In another study[130], superconductivity was induced in gold by molybdenum rhenium pads through the proximity effect to create superconducting nanojunctions. With the insertion of monoradicals, the interplay between Kondo screening and Cooper pair correlations was studied and the presence of Shiba states identified.

[H1] Conclusion and outlook

As discussed above, many examples of exciting quantum-transport phenomena have been demonstrated. Nevertheless, numerous challenges remain, including furthering understanding of how functionality can be built into molecular structure or how it can be optimally exploited. In addition, several factors are still poorly understood, including transport in the regime between weak and strong Coulomb interactions and the transition from coherent to incoherent transport. Moreover, the single-level model is difficult to capture in an experiment. There is thus substantial scope for development, and we briefly discuss four research directions that we believe will become relevant in the near future.

To develop single-molecule electronics, it is crucial to study key molecules in different measurement platforms so that a more complete picture of their properties can be obtained and assessed. As most single-molecule measurements are statistical in nature owing to the different molecular configurations, a more robust analysis that includes all collected data is needed. Data collection should therefore be unbiased and automated; additionally, the full data set should always be presented and analysed using an unsupervised approach (see below). Such a robust analysis is useful, for example, when reporting on molecular switches. Switching may have several underlying mechanisms, some of which are not related to the internal structure of the molecule but could instead be attributable to mechanical instability of the junctions or changes in the electronic coupling between the molecule and the electrodes[131], changes in the electrostatic environment (including the substrate)[132] or the presence of ions that are needed to stabilize the molecule[133].

Although the unambiguous demonstration of molecular functionalities across different experimental platforms remains a challenge, the development of new instrumentation has granted researchers access to large datasets, which can be evaluated using statistical tools such as machine learning. Generally, supervised learning is used when the nature of the desired machine learning model output is known, whereas unsupervised learning is used, for example, to detect the underlying (and unknown) structures of a given dataset. The unsupervised approach has successfully been applied to classify breaking (*G(d)*) curves and conductance histograms into different clusters according to characteristic features[134,135,136]. These examples highlight the importance of developing sophisticated tools to analyse large breaking-trace datasets with the goal to eventually connect the different data clusters to different junction configurations and/or geometries.

A promising and emerging research direction is the study of molecule–light interactions to enable light to be used to read out or manipulate the state of a molecule. In several studies, the electrical DC conductance of a junction has been measured with and without illumination. The challenge of these experiments is the variety of competing optoelectronic mechanisms. Non-linear *I*–*V* characteristics of nanogaps between metallic electrodes can lead to rectification of the AC electric field component of the laser light into a DC photocurrent[137] — a phenomenon known as optical rectification. Illumination can induce geometrical changes in the molecular junctions that alter the conductance. In some metal contacts, such as gold, plasmons can be excited by direct illumination[138] or by using a grating[139,140]. Plasmon decay can generate hot electrons, making it more difficult to disentangle thermal effects from purely optical ones[141,142]. Moreover, molecules can absorb light or electromagnetic waves at other wavelengths, resulting in photon-assisted transport, as recently demonstrated using terahertz radiation[143].

There is an increasing fascination for how nature exploits charge transport in living organisms, and certain biological systems are now known to be efficient conductors of electrical charges, although the underlying mechanisms are not clear[144]. Most experiments have been performed on assemblies of biomolecules; single-molecule studies are rare to date. The complexity of biomolecules brings new opportunities. For example, a biomolecule may not be conjugated over its entire length. Moreover, biomolecules have a high mechanical flexibility, are typically asymmetric with respect to their end groups, have backbones that can contain side groups that act as additional anchoring units to the electrodes, may possess a chiral structure and can adopt different conformations. Moreover, the physical environment (for example, the solvent, pH, ionic strength and temperature) may influence the structure of biomolecules and therefore their transport properties. Although DNA has been studied in break junctions[145], much less is known about amino acids[146], peptide chains[147,148] or single proteins[149].

Over the past two decades, the field of molecular electronics has advanced at a steady pace. Further progress in using more complicated device structures and analysis methods, and in probing poorly explored properties, such as heat and spin transport, molecule–light or molecule–solvent interactions, will reveal new quantum phenomena on the single-molecule level and new possibilities for molecular device functionality.

Acknowledgements
The authors thank The Netherlands Organisation for Scientific Research (NWO) for financial support, including the NWO/OCW Nanofront programme, and acknowledge financial support from the European Union through an advanced European Research Council grant (Mols@Mols), a Future and Emerging Technologies open programme (QuiET (project no. 767187)), a European Cooperation in Science and Technology (COST) Action (MOLSPIN CA15128) and a Marie Curie fellowship (TherSpinMol (ID 748642)). The authors thank M. Perrin and R. Frisenda for discussions.

Author contributions
The authors contributed equally to all aspects of the article.

Competing interests
The authors declare no competing interests.

Publisher's note

Supplementary information
Supplementary information is available for this paper at https://doi.org/10.1038/s415XX-XXX-XXXX-X

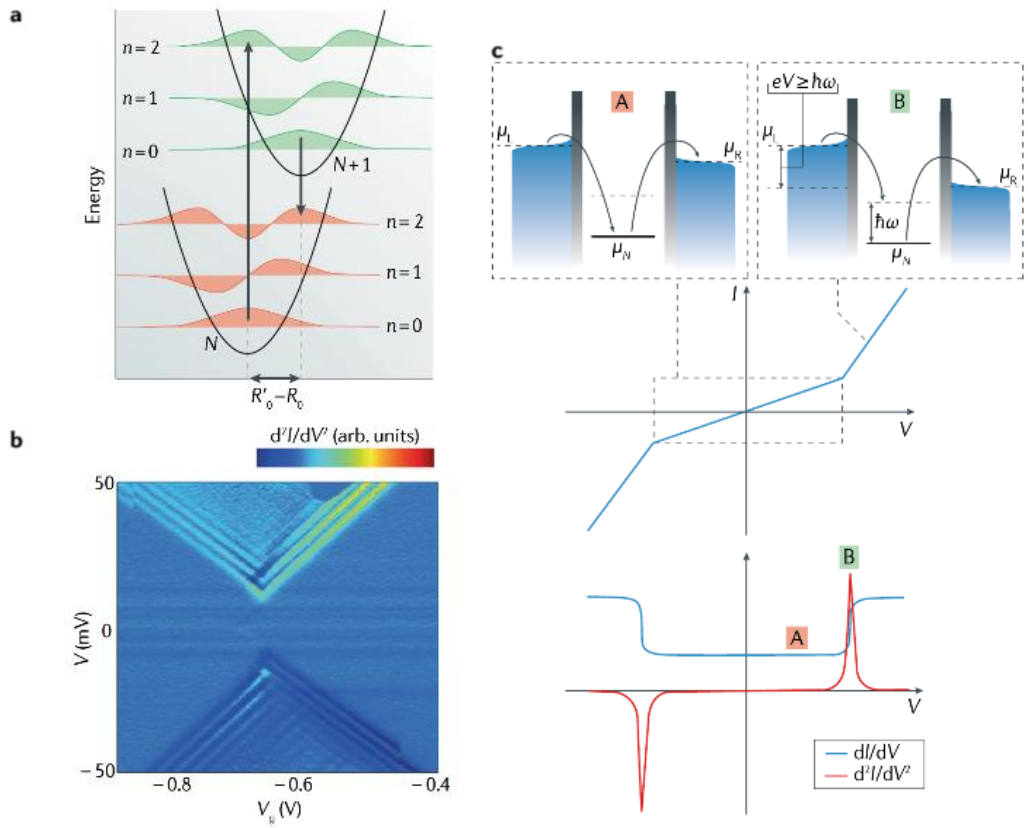

Box 1 **| Vibronic effects**

Electron-transport experiments provide access to the vibrational modes of molecules[150]. When an electron moves through a molecule, it can absorb or release energy to or from the nuclei in the form of vibrational quanta, and thus the single-level model is no longer strictly applicable as the level is now 'dressed' with additional vibrational states.

In the weak coupling limit, the molecule changes its ground-state conformation upon charging or discharging. The charging probability now includes a 'Franck–Condon factor', which has the form $\left|\langle\varphi_n|\varphi'_m\rangle\right|^2$, where φ is the wavefunction, *n* and *m* are the vibrational quantum numbers, and the prime denotes the system in the charged state. Part **a** of the figure shows the Franck–Condon mechanism, in which the two parabolas represent the potential along a vibrational coordinate in two different charge states (*N* is the number of electrons on the molecule), the wavefunctions φ_n and φ_m' correspond to the red and green curves, respectively, and $R'_0 - R_0$ is the shift in the equilibrium position (R_0). Electronic transitions are vertical as they are instantaneous on the timescale of nuclear motion. This Franck–Condon factor is responsible for additional transport features, such as the appearance of additional steps[151] in the current–voltage curve and the possibility for a 'Franck–Condon blockade', which suppresses the current (*I*) at small bias. This phenomenon has been studied theoretically[152] and has been observed in single-molecule transistors[153], as can be seen in part **b** of the figure, which shows an experimental plot of d^2I/dV^2 as a function of the bias voltage (*V*) and gate voltage (V_g) for an Fe_4 complex. At high biases, a harmonic spectrum of equally spaced vibrational excitations is observed.

If the coupling is intermediate, tunnelling processes via a virtual state on the molecule (see part **c** of the figure) are accompanied by a vibrational excitation or de-excitation. Such changes open additional transport channels for the electrons that can be accessed only when the bias voltage exceeds the energy difference between the two vibrational states and lead to an increase in the transmission. This phenomenon is visible as a peak in d^2I/dV^2 (see part **c** of the figure, lower panel),

enabling the identification of vibrational frequencies — a procedure known as inelastic tunnelling spectroscopy[154]. In the very strong coupling regime, emission of vibrational modes can increase backscattering, thereby impeding the current beyond a bias threshold rather than increasing it. Reviews on the experimental features and modelling approaches can be found in ref.[155] and ref.[156], respectively.

μ_L and μ_R, chemical potentials of the left and right electrodes, respectively; μ_N orbital level on the molecule; ω, frequency; e, elementary charge; $\hbar$, reduced Planck's constant. Part **b** of the figure is adapted with permission from ref.[153], American Chemical Society.

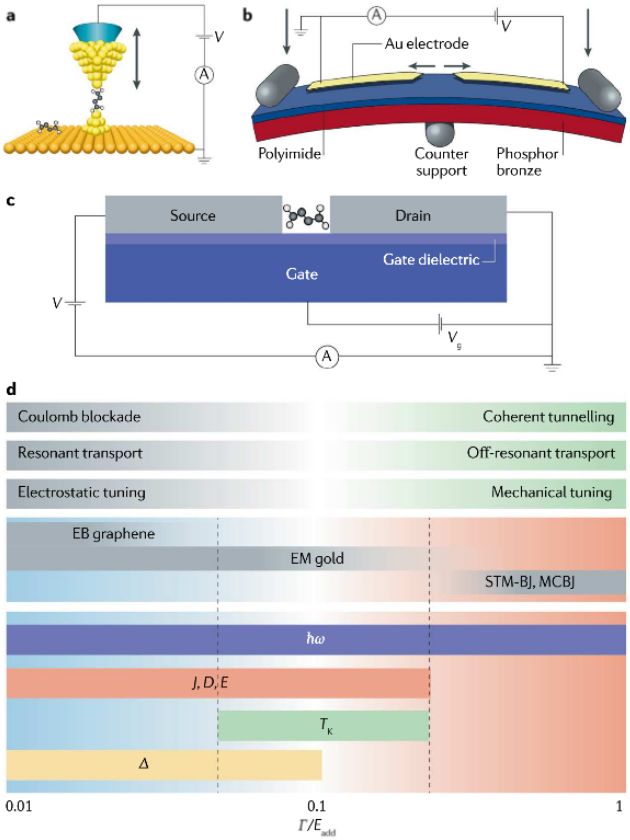

Fig. 1. | **Measurement techniques and transport regimes. a, b** | Two examples of mechanical break junctions. Part **a** shows a scanning tunnelling microscope break junction (STM-BJ). Part **b** shows a mechanically controlled break junction (MCBJ). To determine the conductance of single molecules, a bias voltage (V) is applied to the junction and the resulting current is measured. The black arrows illustrate the direction of mechanical movement. **c** | Electromigrated (EM) break junctions offer gate control (where V_g is the gate voltage) at the expense of collecting multiple-configuration statistics. **d** | Summary of the transport regimes and energy scales at low temperatures (here, a few Kelvin). Whether a certain transport phenomenon can be observed in an experiment mainly depends on the ratio between the tunnel coupling, Γ, and the addition energy, E_{add} (here, a few hundred meV). The accessible tunnel coupling is dictated by the measurement method. Additional energy scales include vibrational energies ($\hbar\omega$, where $\hbar$ is the reduced Planck's constant and ω is the angular frequency), exchange (J), axial (D) and transversal (E) anisotropy energies, the Kondo temperature (T_K) and the superconducting energy gap (Δ). EB, electroburning. Part **a** is adapted with permission from ref.[157], Elsevier. Part **b** is adapted from ref.[56], Springer Nature Limited. Part **c** is adapted with permission from ref.[158], RSC.

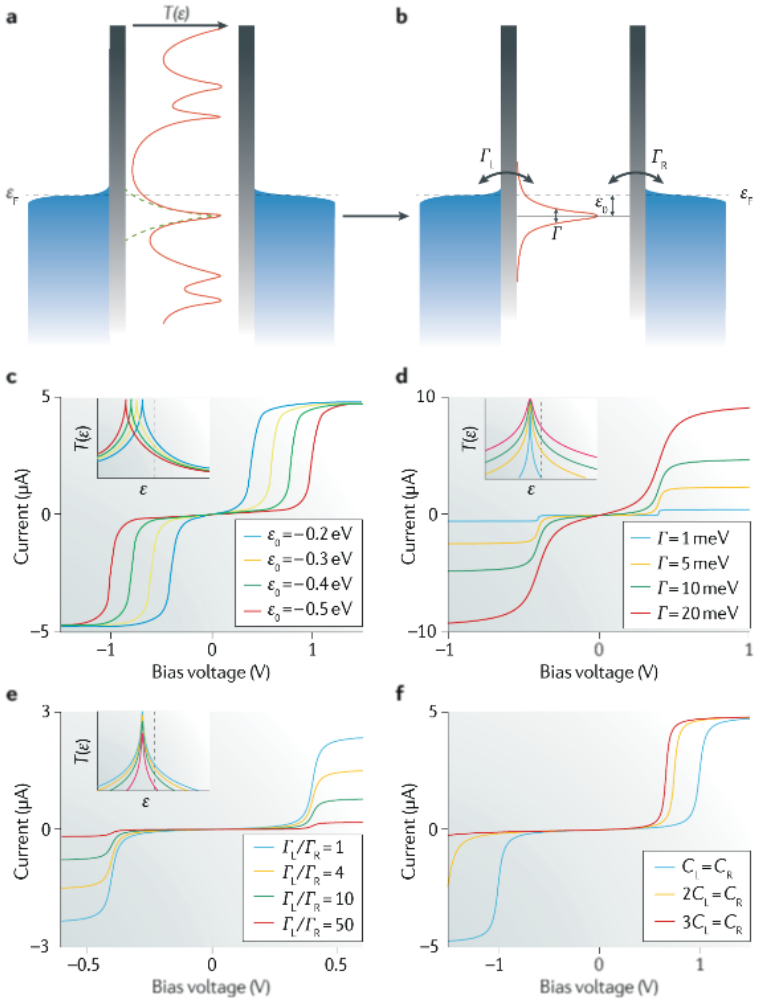

Fig. 2 | **Single-level model in the coherent transport regime. a** | Chemical potential landscape of a molecular junction at zero bias. The density of states of the metal is assumed constant, and the occupation probability is given by Fermi–Dirac statistics (the blue shaded area depicts the occupied states). The probability that an electron with energy ε transmits the molecule is given by the transmission function, $T(\varepsilon)$ (shown in orange). The transmission often resembles the local density of states between the two electrodes; however, there may be resonances in the local density of states that are almost completely decoupled from the electrodes and hence do not show up in the transmission. The orbital closest to the Fermi energy, ε_F, often dominates the transport characteristics (indicated here by the green dashed lines with a Lorentzian peak shape as a first approximation of the transmission). **b** | In the single-level model, the current (I) through a junction is estimated using the orbital level (ε_0) closest to ε_F and the total tunnel coupling Γ, where $\Gamma = \Gamma_L + \Gamma_R$ and Γ_L and Γ_R are the tunnel couplings between the orbital and the left and right electrode, respectively. **c** | I–V (where V is the bias voltage) curves for $\Gamma_L = \Gamma_R = 10$ meV for different values of ε_0 (see inset; the dashed line corresponds to $\varepsilon_F = 0$). There is a low current at low bias with a differential conductance $\frac{dI}{dV} \approx G_0 T(\varepsilon_F)$ (where G_0 is the conductance quantum). At a bias of $eV = 2\varepsilon_0$ (where e is the elementary charge), the current saturates to a level determined by the tunnel couplings (equation 3). As ε_0 approaches ε_F, the zero-bias conductance increases and there is an earlier current onset. **d** | By reducing Γ, $T(\varepsilon)$ becomes sharper (inset) as Γ equals the full width at half maximum of the Lorentzian transmission peak. The constant current level at high bias is reduced and there is a smaller step in current at $eV = 2\varepsilon_0$ (here, $\varepsilon_0 = -0.2$ eV). **e** | Making Γ asymmetric reduces the amplitude of $T(\varepsilon)$ and the saturation current (calculated here for $\varepsilon_0 = -0.2$ eV and $\Gamma = 10$ meV) . Note that the I–V curves are still symmetric. **f** | Making the capacitive coupling asymmetric (C_L and C_R are

the capacitive couplings for the left and right electrodes, respectively) results in asymmetric, diode-like *I–V* characteristics (equation 2, calculated here for $\Gamma_L = \Gamma_R = 10$ meV and $\varepsilon_0 = -0.5$ eV).

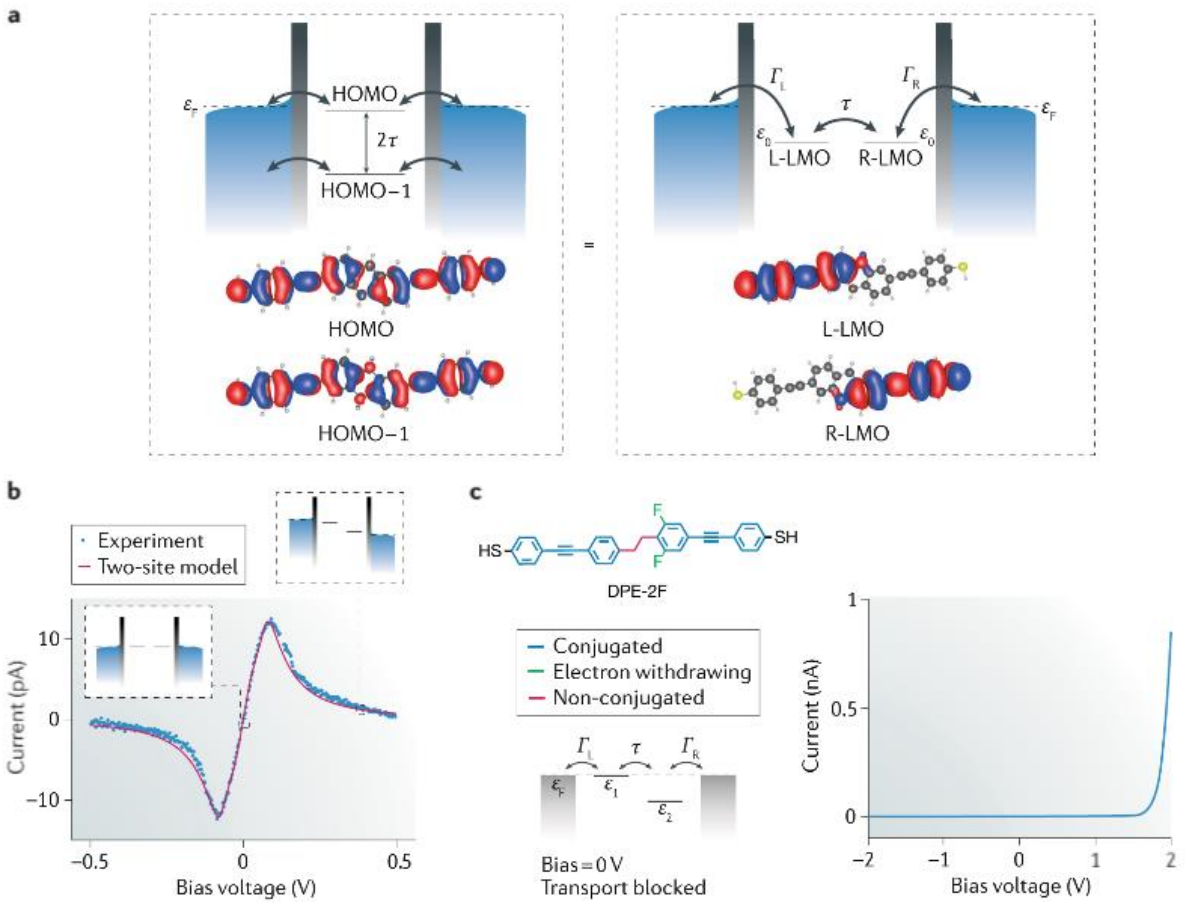

Fig. 3 | **The two-level model. a** | The energy-basis (top, left panel) and site-basis (top, right panel) representation of the two-site model are equivalent. The energy gap 2τ (where τ is the tunnel coupling) between the highest occupied molecular orbital (HOMO) and HOMO – 1 (bottom, left panel) can be interpreted as the energy difference between a bonding and antibonding state that result from the hybridization of two localized molecular orbitals (LMOs) (bottom, right panel). These LMOs are localized on the left (L) and right (R) halves of a single molecule owing to broken conjugation in the molecular backbone. As an example, the HOMO and HOMO – 1 orbitals and corresponding L-LMO and R-LMO of 9,10-dihydroanthracene are shown. Moving from one representation to the other corresponds to a basis transformation; calculations in these bases are equivalent and yield, for example, the same current–voltage characteristics. **b** | Negative differential resistance (NDR) behaviour of 9,10-dihydroanthracene molecules. The two-site model can be used to fit the experimental data. The two sites in series representations (insets) provide an intuitive explanation for the observed NDR. At zero bias, the two sites are resonant and tunnelling between them is possible. By applying a high bias voltage, the two sites detune, reducing the tunnel coupling and consequently the current through the junction. **c** | Diode-like behaviour in a DPE-2F molecule. The on-site energies of the left (ε_1) and right (ε_2) LMOs (that is, the energies needed to put an electron into these LMOs) are different owing to functionalization of one of the subunits; therefore, at zero bias, transport is blocked (bottom, left panel). The level alignment can be tuned by applying a bias, which results in alignment and an increase in current) (right panel) or misalignment depending on the sign of the bias voltage. ε_0, energy of the orbital closest to the Fermi level (ε_F). Γ_L and Γ_R, tunnel couplings to the left and right electrodes, respectively. Parts **a** and **b** are adapted from ref.[56], Springer Nature Limited. Part **c** is adapted from ref.[58], CC-BY-3.0.

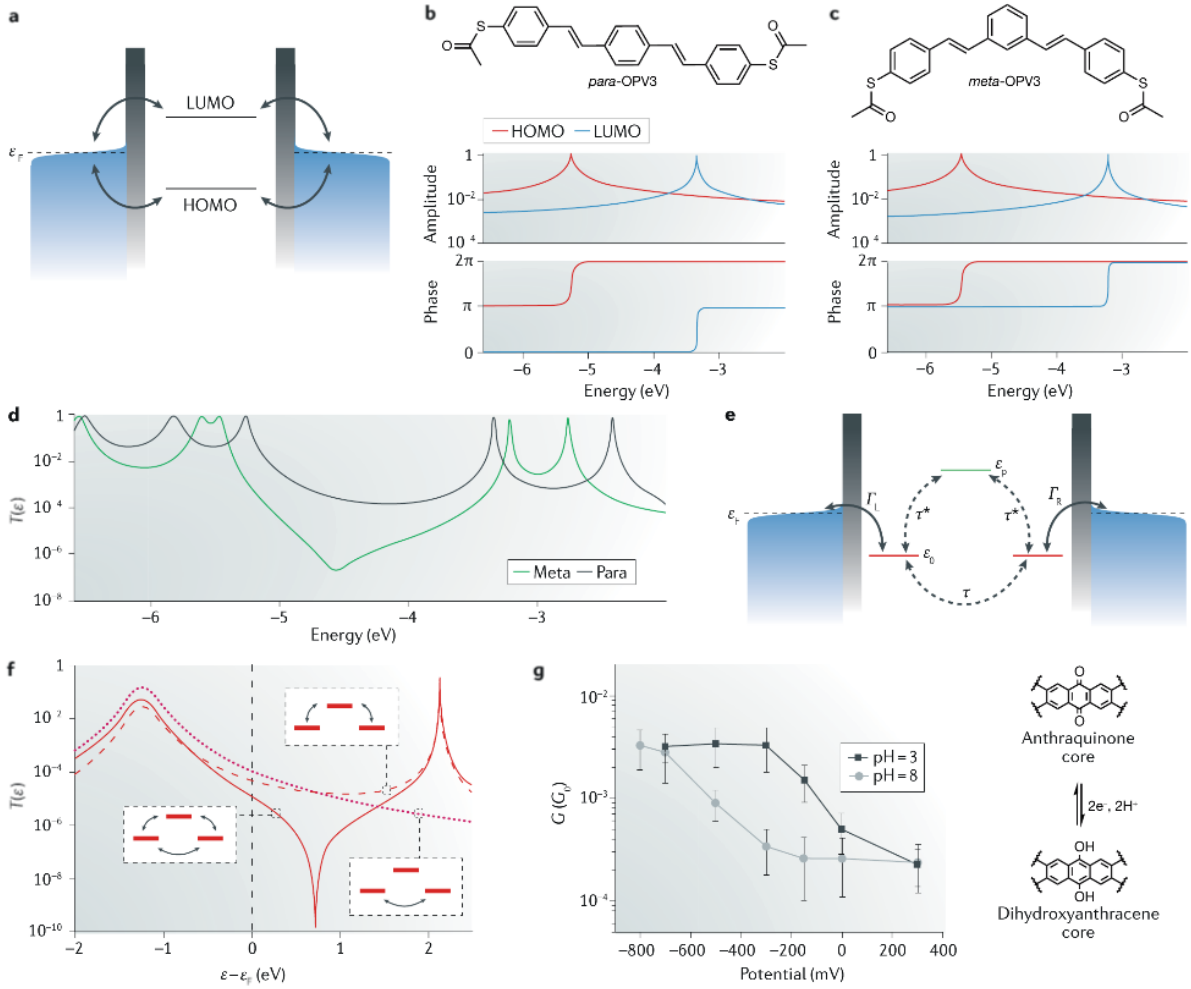

Fig. 4 | **Quantum interference in molecular junctions. a |** Quantum interference occurs when the transmission through different molecular orbitals are combined (here, the highest occupied molecular orbital (HOMO) and lowest unoccupied molecular orbital (LUMO)). As contributions from different orbitals have amplitude and phase, they interfere constructively or destructively. **b** | Amplitude and phase of the transmission through the HOMO and LUMO of *para*-oligo(3)-phenylenevinylene (OPV3). **c** | Amplitude and phase of the transmission through the HOMO and LUMO of *meta*-OPV3. **d** | Calculated transmission function ($T(\varepsilon)$) through the π systems of *meta*-OPV3 and *para*-OPV3. **e** | Interference between a direct transmission path (through a delocalized orbital with energy ε_0, red states) and a transmission path via a pendant state (a localized orbital with energy ε_p that couples to the delocalized orbital but not to the electrodes, green state). τ is the tunnel coupling between the delocalized states, τ^* is the tunnel coupling between the delocalized and localized states, and Γ_L and Γ_R are the tunnel couplings to the left and right electrodes, respectively. **f** | $T(\varepsilon)$ with asymmetric features. Direct transmission through the backbone (dotted line) or a localized state (dashed line) give rise to transmission resonances. The interference between the pathways results in a transmission dip in the total $T(\varepsilon)$ (solid line). **g** | Destructive quantum interference strongly suppresses conductance (G) in cross-conjugated anthraquinone. Destructive quantum interference can be switched off by reducing the molecule through electrochemical gating or by changing the pH of the solution, leading to the formation of linearly conjugated dihydroxyanthracene. ε, energy; ε_F, Fermi energy; G_0, conductance quantum. Parts **b**–**d** are adapted from ref.[60], CC-BY-2.0. Part **f** is adapted from ref. [159], Springer Nature Limited. Part **g** is adapted with permission from ref.[68], Wiley-VCH.

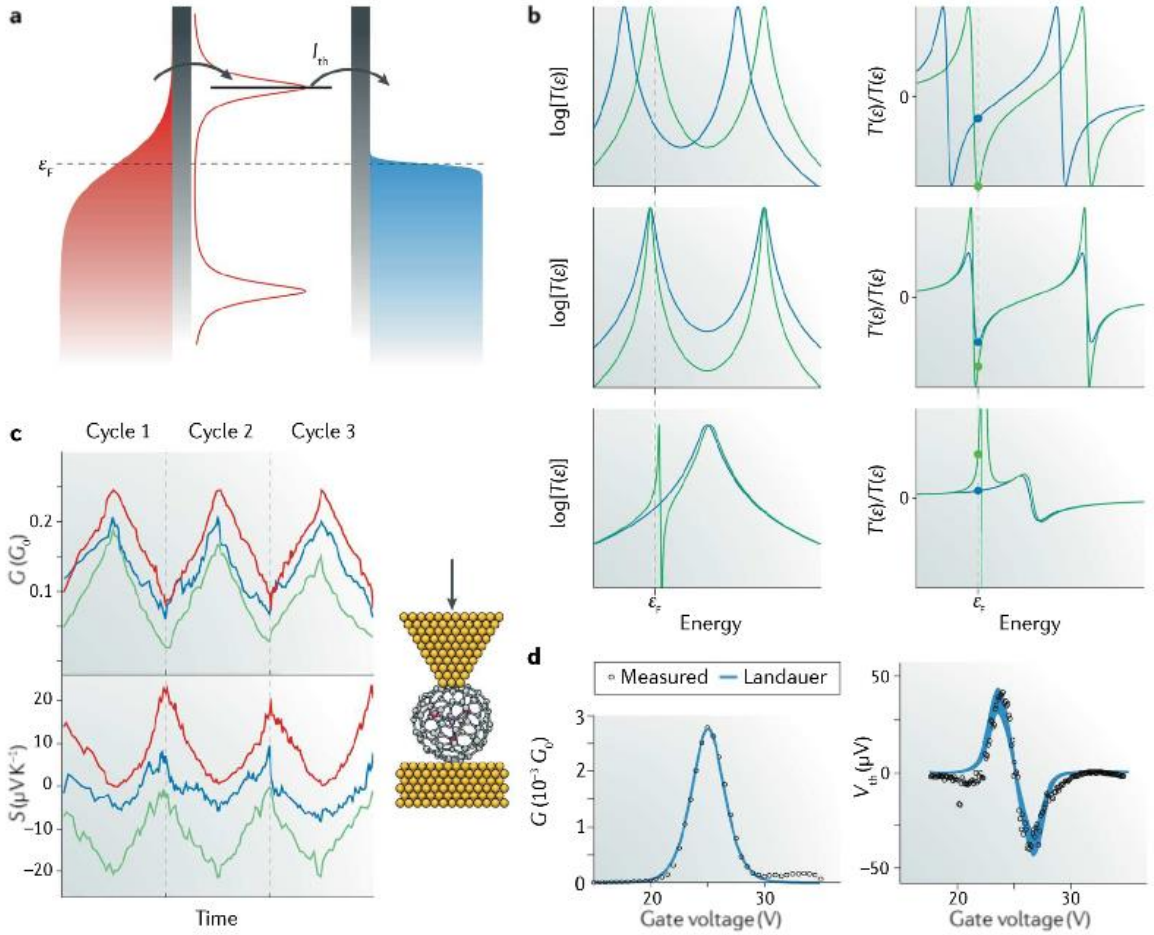

Fig. 5 | **Thermoelectric effects in molecular junctions. a** | Level diagram showing the creation of a thermal current, I_{th}, when one side of the junction is heated (depicted by the broadened, red Fermi–Dirac distribution). **b** | Different ways to increase the Seebeck coefficient, S (where $S \propto T'(\varepsilon)/T(\varepsilon)$, and $T(\varepsilon)$ is the transmission function), in molecular junctions (right panels). As S depends on the local slope of $T(\varepsilon)$ (left panels) at the Fermi energy (ε_F), it can be increased by moving resonances closer to ε_F (top panels), by reducing the tunnel coupling (middle panels) or by introducing sharp resonance features (bottom panels). These enhancements are depicted as the transition from the blue to the green points. **c** | Mechanical control of thermoelectricity. The conductance (G, top, left panel) and S as a function of mechanical deformation of a $Sc_3N@C_{80}$ molecule measured using a scanning tunnelling microscopy break junction (right panel). The incorporation of Sc_3N clusters leads to an additional resonance close to ε_F; the position of this resonance can be tuned by compressing the molecule. **d** | Gate control of thermoelectricity in molecular junctions. Comparison of experimental and calculated gate-dependent G (left panel) and thermovoltage (V_{th}, right panel) of a C_{60} molecule contacted with graphene electrodes. G_0, conductance quantum. Part **c** is adapted from ref.[88], Springer Nature Limited. Part **d** is adapted from ref.[90], ACS.

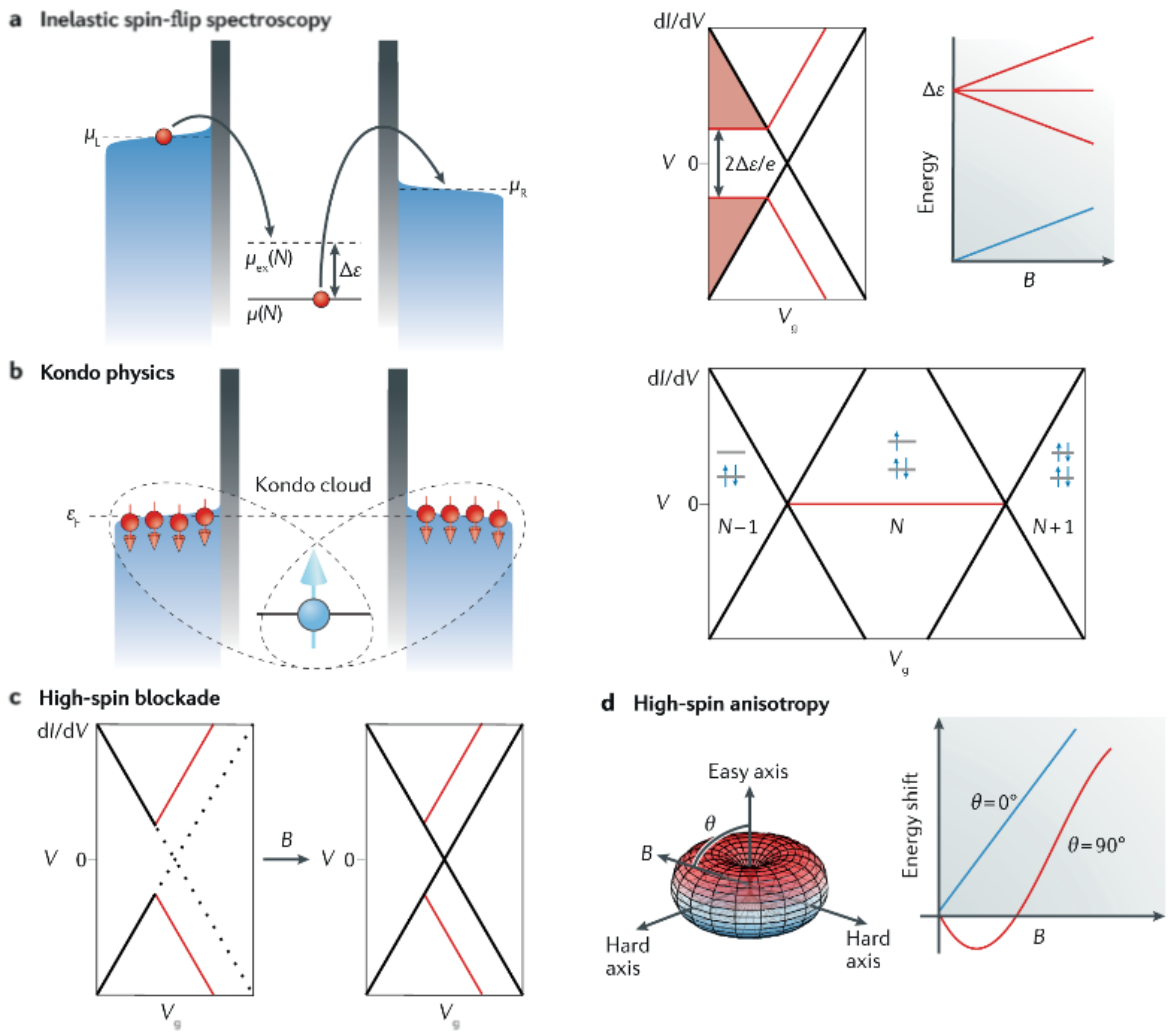

Fig. 6 | **Spin-dependent effects in molecular junctions. a** | The left panel shows inelastic co-tunnelling, a second-order process involving a ground state with chemical potential $\mu(N)$ and an excited state at chemical potential $\mu_{ex}(N)$. Inelastic co-tunnelling occurs when the energy difference $\Delta\varepsilon = \mu_{ex}(N) - \mu(N)$ is supplied by the applied bias voltage (V) and results in a region with finite differential conductance (red shaded area in the middle panel) inside the Coulomb-blocked regime indicated by the white regions outside the hourglass defined by the black lines. In this plot of the differential conductance as a function of gate voltage (V_g) and V, these black lines indicate the onset of the sequential tunnelling contribution to the current; the red lines correspond to the onset of that of the excited state. Co-tunnelling spectroscopy can be used to analyse the ground and excited states. For example, a transition between a spin-1/2 ground state and a spin-3/2 excited state is shown (right panel). There is three-fold splitting (red lines) starting at $eV = \Delta\varepsilon$ (where e is the elementary charge) at zero magnetic field (B) owing to the transitions to the excited multiplet. The ground-state doublet at $B = 0$ yields a sloped line (blue) starting at $V = 0$ due to Zeeman splitting. **b** | The Kondo effect (left panel) originates from the formation of a many-body spin singlet between the spin residing on the molecule and the conduction electrons, leading to screening within the Kondo length ζ_K (that is, formation of a 'Kondo screening cloud'). These Kondo correlations result in a resonance in the density of states of the system pinned to the Fermi energy (ε_F). Thus, a peak in the differential conductance around zero bias can be observed (red line in the plot of dI/dV, right panel) if the molecule is occupied by an odd number (N) of electrons (that is, with a total spin of 1/2). **c** | Spin-blockade in the single-electron tunnelling regime. If the ground-state transition is spin forbidden (that is, if $|S_{N+1} - S_N| > 1/2$, where S is the spin angular momentum) transport at low V is blocked for all values of V_g (the dotted lines denote conductance steps completely suppressed by spin blockade).

The blockade can be lifted if either a spin-allowed excited state can be accessed through *V* (red solid lines) or if an external magnetic field is used to induce a spin transition of the ground state (right panel). **d** | Application of single-electron tunnelling spectroscopy to identify single-molecule magnetic behaviour. The left panel shows the energy needed to align a spin along certain directions in a single-molecule magnet using an external magnetic field. The right panel shows that the energy shift of charge degeneracy points depends on the angle (θ) between *B* and the easy axis.

Table 1 | **Comparison of break-junction techniques**

Break junction	Multiple configuration statistics?	Low-bias junction lifetime	Operation temperature	Electrode configuration	Gate (level shifts)	Main operation modes[a]
STM-BJ	Yes	<0.1–10 s	Room temperature	Asymmetric	Electrochemical in liquid (±0.75 eV)	$G(d)$[b], I–$V(d,t)$, $F(d)$
MCBJs	Yes	>100 s	0.1–300 K	Symmetric	Solid state (±0.05 eV)	$G(d)$[b], I–$V(d,t)$, IETS(d)
Electromigrated break junctions	No	Days	• Gold: <200 K • Graphene: 0.1–300 K	Symmetric	Solid state (±0.25 eV)	I–$V(V_g,B,T,t)$

MCBJ, mechanically controlled break junction; STM-BJ, scanning tunnelling microscopy break junction. [a]The operating modes include conductance (G) versus displacement (d) measurements; the measurement of current–voltage (I–V) characteristics either during stretching as a function of d or time (t) for a fixed distance, in which the capture of a molecule appears as a sudden increase in G; the simultaneous measurement of force (F) versus d; and inelastic-tunnelling spectroscopy (IETS) measurements, which are typically performed at low temperatures. For electromigrated junctions, detailed spectroscopy as a function of gate voltage (V_g), magnetic field (B) and temperature (T) is used. [b]Owing to the drift in the tip position in STM-BJ set-ups at room temperature, special care has to be taken to probe the full stretching of the molecule. In some cases, $G(d)$ curves show only a very limited displacement range (which is not related to the molecular length even when correcting for the 'snap-back' effect, which for gold electrodes in both mechanical break junction set-ups adds ~0.5 nm to the displacement axis), making it more difficult to establish the molecular configuration.

Glossary terms

Coulomb blockade
Phenomenon in which the Coulomb interactions on a molecule in a junctionare strong enough to prevent electrons from entering or leaving the molecule.

Incoherent transport
Transport in which the electronic wavefunction is perturbed (typically by the electrostatic field of the nuclei).

Coherent transport
Transport in which the electronic wavefunction is not perturbed by the environment.

Off-resonant transport
Transport via a molecular orbital with a chemical potential that does not lie between those of the left and right electrode.

Resonant transport
Transport via a molecular orbital with a chemical potential that lies between those of the left and right electrode.

Superconducting gap
Minimum excitation energy for electrons in a superconductor

Physisorption
Coupling between a molecule and a solid through van der Waals interactions.

Chemisorption
Coupling between a molecule and a solid through chemical bonding.

Orbital levels
Chemical potentials associated with the addition or removal of an electron to or from molecular orbitals.

Chemical potential
Energy difference between a molecule with a particular orbital filled by an electron and the same molecule in which that orbital is empty.

Fermi energy
Chemical potential (of the electrodes) at zero absolute temperature.

Fowler–Nordheim tunnelling
Tunnelling process in which electrons are extracted from a metal using a strong electric field.

Proximity effect
Phenomenon in which the proximity of a superconductor induces superconductivity in a material which by itself in not superconducting.

References

1 Cuevas, J. C. & Scheer, E. Molecular Electronics: An Introduction to Theory and Experiment, *World Scientific, Singapore* (2017).
2 Ratner, M.A. A brief history of molecular electronics. *Nature Nanotechnology* **8**, 378-381 (2013).
3 Tsutsui, M. & Taniguchi, M. Single Molecule Electronics and Devices. *Sensors* **12**, 7259–7298 (2012).
4 Lörtscher, E. Wiring molecules into circuits. *Nature Nanotechnology* **8**, 381–384 (2013).
5 Sun, L. et al. Single-molecule electronics: from chemical design to functional devices. *Chem. Soc. Rev.* **43** 7378-7411 (2014).
6 Metzger, R.M. Unimolecular Electronics. *Chem. Rev.* **115**, 5056–5115 (2015).
7 Su, T., Neupane, M., Steigerwald, M., Venkataraman, L. & Nuckolls, C. Chemical principles of single-molecule electronics. *Nature Reviews Materials* **1**, 16002 (2016).
8 Xiang, D., Wang, X., Jia, C., Lee, T. & Guo, X. Molecular-Scale Electronics: From Concept to Function. *Chem. Rev.* **116**, 4318-4440 (2016).
9 Xin, N., *et al.* Concepts in the design and engineering of single-molecule electronic devices. *Nature Reviews Physics* **1**, 211-230 (2019).
10 Perrin, M. L., Burzurí, E., van der Zant, H. S. J. Single-molecule transistors. *Chem. Soc. Rev.* **44**, 902-919 (2015).
11 Van der Molen, S. J. & Liljeroth, P. Charge transport through molecular switches. *J. Phys.* **22**, 133001 (2010).
12 Capozzi, B. *et al*. Single-molecule diodes with high rectification ratios through environmental control. *Nature Nanotechnology* **10**, 522–527 (2015).
13 Trasobares, J., Vuillaume, D., Théron, D. & Clément, N. A 17 GHz molecular rectifier. *Nature Communications* **7**, 12850 (2016).

14 Aragonès, A.C., Darwish, N., Ciampi, S., Sanz, F., Gooding., J.J., & Díez-Pérez, I. Single-molecule electrical contacts on silicon electrodes under ambient conditions. *Nature Communications* **8**, 15056 (2017).
15 Perrin, M.L., Doelman, M., Eelkema, R. & van der Zant, H.S.J. Design of an efficient multi-site single-molecule rectifier. *Physical Chemistry Chemical Physics* **19**, 29187–29194 (2017).
16 Smit, R.H.M., *et al.* Measurement of the conductance of a hydrogen molecule. *Nature* **419**, 906-909 (2002).
17 Xu, B. & Tao, N.J. Measurement of Single-Molecule Resistance by Repeated Formation of Molecular Junctions. *Science* **301**, 1221-1223 (2003).
18 Hybertsen, M. S.; Venkataraman, L., Structure–property relationships in atomic-scale junctions: Histograms and beyond. *Accounts of chemical research* **2016**, *49*, 452-460.
19 Van Ruitenbeek, J.M., Alvarez, A., Pineyro, I., Grahmann, C., Joyez, .P, Devoret, M.H, Estéve, D. & Urbina, C. Adjustable nanofabricated atomic size contacts. *Rev. Sci. Instrum*. **67**, 108-111 (1996).
20 Wang, L., Wang, L., Zhang, L. & Xiang, D. Advance of Mechanically Controllable Break Junction for Molecular Electronics. *Topics in Current Chemistry* **375**, 61 (2017).
21 Aradhya, S. V. & Venkataraman, L. Single-molecule junctions beyond electronic transport. *Nature Nanotechnology* **8**, 399-410 (2013).
22 Huang, C., Rudnev, A.V., Hong, W., & Wandlowski, T. Break junction under electrochemical gating: testbed for single-molecule electronics. *Chem. Soc. Rev.* **44**, 889–901 (2015).
23 Martin, C.A., van Ruitenbeek, J.M. & van der Zant, H. S. J. Sandwich-type gated mechanical break junctions. *Nanotechnology* **21**, 265201 (2010).
24 Arima, A. et al. Fabrications of insulator-protected nanometer-sized electrode gaps. *Journal of Applied Physics* **115**, 114310 (2014).
25 Muthusubramanian, N. et al. Insulator-protected mechanically controlled break junctions for measuring single-molecule conductance in aqueous environments. *Appl. Phys. Lett.* **109**, 013102 (2016).
26 Bellunato, A. et al. Dynamic Tunneling Junctions at the Atomic Intersection of Two Twisted Graphene Edges. *Nano Lett.* **18**, 2505-2510 (2018).
27 Caneva, S. et al. Mechanically controlled quantum interference in graphene break junctions. Nature Nanotechnology (2018), DOI: 10.1038/s41565-018-0258-0.
28 Park, H., Lim, A.K.L, Alivisatos, A.P., Park, J. & McEuen, P.L. Fabrication of metallic electrodes with nanometer separation by electromigration. *Appl. Phys. Lett.* **75**, 301 (1999).
29 Strachan, D.R. et al., Controlled fabrication of nanogaps in ambient environment for molecular electronics, *Appl. Phys. Lett.* **86**, 043109 (2005).
30 O'Neill, K., Osorio, E.A. & van der Zant, H.S.J. Self-breaking in planar few-atom Au constrictions for nanometer-spaced electrodes. *Appl. Phys. Lett.* **90** 133109 (2007).
31 Prins, F. et al. Room-Temperature Gating of Molecular Junctions Using Few-Layer Graphene Nanogap Electrodes. *Nano Lett.*, **11**, 4607-4611 (2011).
32 Candini, A. et al. Electroburning of few-layer graphene flakes, epitaxial graphene, and turbostratic graphene discs in air and under vacuum. *Beilstein J. Nanotechnol.*, **6**, 711-719 (2015).
33 Lau, C. S., Mol, J. A., Warner, J. H., Briggs, G. A. D. Nanoscale control of graphene electrodes. *Phys. Chem. Chem. Phys.*, **16**, 20398-20401 (2014).
34 El Abbassi, M. et al. *Nanoscale*, **9**, 17312-17317 (2017).
35 Barreiro, A., van der Zant, H. S., Vandersypen, L. M. Quantum dots at room temperature carved out from few-layer graphene. *Nano Lett.*, **12** , 6096-100 (2012).
36 Gehring, P. et al. Quantum Interference in Graphene Nanoconstrictions. *Nano Lett.*, **16**, 4210-4216 (2016).
37 Jia, C. & Guo, X. Molecule–electrode interfaces in molecular electronic devices. *Chem. Soc. Rev.* **42**, 5642-5660 (2013).

38 Leary, E., La Rosa, A., González, M.T., Rubio-Bollinger, G., Agraït, N. & Martín, N. Incorporating single molecules into electrical circuits. The role of the chemical anchoring group. *Chem. Soc. Rev.* **44**, 920-42 (2015).
39 Dubois, V., Raja, S.N., Gehring, P., Caneva, S., van der Zant, H.S.J., Niklaus, F. & Stemme G. Massively parallel fabrication of crack-defined gold break junctions featuring sub-3 nm gaps for molecular devices. *Nature Communications* **9**, 3433 (2018).
40 Ishii, H. et al. Energy level alignment and band bending at model interfaces of organic electroluminescent devices. *J. Lumin.* **61**, 87–89 (2000).
41 Datta, S. Electronic Transport in Mesoscopic Systems, Cambridge University Press, Cambridge (1995); doi:10.1017/CBO9780511805776.
42 Thijssen, J.M. & van der Zant, H.S.J. Charge transport and single-electron effects in nanoscale systems. *Phys. stat. sol. (b)* **245,** 1455-1470 (2008).
43 Hanson, R. et al. Spins in few-electron quantum dots. *Rev. Mod. Phys.* **79**, 1217 (2007).
44 Hou, J. G. et al. Nonclassical Behavior in the Capacitance of a Nanojunction. *Phys. Rev. Lett.* **86**, 5321 (2001).
45 Taylor, J. et al. Theory of Rectification in Tour Wires: The Role of Electrode Coupling. *Phys. Rev. Lett.* **89**, 138301 (2002).
46 Li, H. et al., Electric Field Breakdown in Single Molecule Junctions. *J. Am. Chem. Soc.* **137**, 5028–5033 (2015).
47 Foti, G. & Vázquez, H. J. Origin of Vibrational Instabilities in Molecular Wires with Separated Electronic States. *Phys. Chem. Lett.* **9**, 2791–2796 (2018).
48 Beebe, J. M., Kim, B. S., Gadzuk, J., Frisbie, C.D. & Kushmerick, J.G. Transition from Direct Tunneling to Field Emission in Metal-Molecule-Metal Junctions. *Phys. Rev. Lett.* **97**, 026801 (2006).
49 Mirjani, F., Thijssen, J.M. & van der Molen, S.J. Advantages and limitations of transition voltage spectroscopy: A theoretical analysis. *Phys Rev B.* **84**, 115402 (2011).
50 Vilan, A. Revealing tunnelling details by normalized differential conductance analysis of transport across molecular junctions, *Phys. Chem. Chem. Phys.* **19**, 27166–27172 (2017).
51 Capozzi, B. et al. Mapping the Transmission Functions of Single-Molecule Junctions. *Nano Lett.* **16**, 3949-3954 (2016).
52 Frisenda, R., & van der Zant, H. S. J. Transition from strong to weak electronic coupling in a single-molecule junction, *Phys. Rev. Lett.* **117,** 126804 (2016).
53 Lovat, G. et al. Room-temperature current blockade in atomically defined single-cluster junctions. *Nature Nanotechnology* **12**, 1050-1054 (2017).
54 Yuan, L. et al. Transition from direct to inverted charge transport Marcus regions in molecular junctions via molecular orbital gating. *Nature Nanotechnology* **13**, 322–329 (2018).
55 Sowa, J. K. et al. Beyond Marcus theory and the Landauer-Büttiker approach in molecular junctions: A unified framework. *The Journal of Chemical Physics* **149**, 154112 (2018).
56 Perrin, M. L. et al. Large negative differential conductance in single-molecule break junctions. *Nature Nanotechnology* **12**, 830–834 (2014).
57 Perrin, M. L. et al. Single-Molecule Resonant Tunneling Diode. *J. Phys. Chem. C* **119**, 5697–5702 (2015).
58 Perrin, M. L. et al. A gate-tunable single-molecule diode. *Nanoscale* **8**, 8919-8923 (2016).
59 Arroyo, C. et al. Signatures of Quantum Interference Effects on Charge Transport Through a Single Benzene Ring. *Angewandte Chemie International Edition* **52**, 3152-3155 (2013).
60 Arroyo, C. et al. Quantum interference effects at room temperature in OPV-based single-molecule junctions. *Nanoscale Research Letters* **8**, 234 (2013).
61 Manrique, D. et al. A quantum circuit rule for interference effects in single-molecule electrical junctions. *Nature Communications* **6**, 6389 (2015).
62 Geng, Y. et al. Magic Ratios for Connectivity-Driven Electrical Conductance of Graphene-like Molecules. *Journal of the American Chemical Society* **137**, 4469-4476 (2015).

63 Valkenier, H. et al. Cross-conjugation and quantum interference: a general correlation?. *Phys. Chem. Chem. Phys.* **16**, 653-662 (2014).
64 Vazquez, H. et al. Probing the conductance superposition law in single-molecule circuits with parallel paths. *Nature Nanotechnology* **7**, 663-667 (2012).
65 Garner, M. et al. Comprehensive suppression of single-molecule conductance using destructive σ-interference. *Nature* **558**, 415-419 (2018).
66 Liu, X. et al. Gating of Quantum Interference in Molecular Junctions by Heteroatom Substitution. *Angewandte Chemie International Edition* **56**, 173-176 (2016).
67 Koole, M., Thijssen, J., Valkenier, H., Hummelen, J. & van der Zant, H.S.J. Electric-Field Control of Interfering Transport Pathways in a Single-Molecule Anthraquinone Transistor. *Nano Letters* **15**, 5569-5573 (2015).
68 Darwish, N. et al. Observation of Electrochemically Controlled Quantum Interference in a Single Anthraquinone-Based Norbornylogous Bridge Molecule. *Angewandte Chemie International Edition* **51**, 3203-3206 (2012).
69 Li, Y. et al., Gate controlled quantum interference: direct observation of anti-resonances in single molecule charge transport. *Nature Materials* 18, 357 – 363 (2019).
70 J. Bai et al., Anti-resonance features of destructive quantum interference in single-molecule thiophene junctions achieved by electrochemical gating. *Nature Materials* 18, 364 – 369 (2019).
71 Frisenda, R., Janssen, V.E.A.C., Grozema, F.C., van der Zant, H.S.J. & Renaud, N. Mechanically controlled quantum interference in individual π-stacked dimers. *Nature Chemistry* **8**, 1099-1104 (2016).
72 Stefani, D. et al. Large Conductance Variations in a Mechanosensitive Single-Molecule Junction. *Nano Lett.* (2018), DOI: 10.1021/acs.nanolett.8b02810.
73 Markussen, T. Phonon interference effects in molecular junctions. J. Chem. Phys. **139**, 244101 (2013).
74 Finch, C., García-Suárez, V. & Lambert, C. Giant thermopower and figure of merit in single-molecule devices. *Physical Review B* **79**, 033405 (2009).
75 Lambert, C. Basic concepts of quantum interference and electron transport in single-molecule electronics. *Chemical Society Reviews* **44**, 875-888 (2015).
76 Lambert, C., Sadeghi, H. & Al-Galiby, Q. Quantum-interference-enhanced thermoelectricity in single molecules and molecular films. *Comptes Rendus Physique* **17**, 1084-1095 (2016).
77 Paulsson, M. & Datta, S. Thermoelectric effect in molecular electronics. *Physical Review B* **67**, 241403(R) (2003).
78 Good review: Rincón-García, L., Evangeli, C., Rubio-Bollinger, G. & Agraït, N. Thermopower measurements in molecular junctions. *Chemical Society Reviews* **45**, 4285-4306 (2016).
79 Widawsky, J., Darancet, P., Neaton, J. & Venkataraman, L. Simultaneous Determination of Conductance and Thermopower of Single Molecule Junctions. *Nano Letters* **12**, 354-358 (2011).
80 Evangeli, C. et al. Engineering the Thermopower of C60 Molecular Junctions. *Nano Letters* **13**, 2141-2145 (2013).
81 Morikawa, T., Arima, A., Tsutsui, M. & Taniguchi, M. Thermoelectric voltage measurements of atomic and molecular wires using microheater-embedded mechanically-controllable break junctions. *Nanoscale* **6**, 8235-8241 (2014).
82 Reddy, P., Jang, S., Segalman, R. & Majumdar, A. Thermoelectricity in Molecular Junctions. *Science* **315**, 1568-1571 (2007).
83 Malen, J. et al. Identifying the Length Dependence of Orbital Alignment and Contact Coupling in Molecular Heterojunctions. *Nano Letters* **9**, 1164-1169 (2009).
84 Baheti, K. et al. Probing the Chemistry of Molecular Heterojunctions Using Thermoelectricity. *Nano Letters* **8**, 715-719 (2008).
85 Pauly, F., Viljas, J. K. & Cuevas, J. C. Length-dependent conductance and thermopower in single-molecule junctions of dithiolated oligophenylene derivatives: A density functional study. *Phys. Rev. B* **78**, 035315 (2008).

86 Widawsky, J., Darancet, P., Neaton, J. & Venkataraman, L. Simultaneous Determination of Conductance and Thermopower of Single Molecule Junctions. *Nano Letters* **12**, 354-358 (2011).
87 Yee, S., Malen, J., Majumdar, A. & Segalman, R. Thermoelectricity in Fullerene–Metal Heterojunctions. *Nano Letters* **11**, 4089-4094 (2011).
88 Rincón-García, L. et al. Molecular design and control of fullerene-based bi-thermoelectric materials. *Nature Materials* **15**, 289-293 (2015).
89 Kim, Y., Jeong, W., Kim, K., Lee, W. & Reddy, P. Electrostatic control of thermoelectricity in molecular junctions. *Nature Nanotechnology* **9**, 881-885 (2014).
90 Gehring, P. et al. Field-Effect Control of Graphene–Fullerene Thermoelectric Nanodevices. *Nano Letters* **17**, 7055-7061 (2017).
91 Lee, W. et al. Heat dissipation in atomic-scale junctions. *Nature* **498**, 209-212 (2013).
92 Cui, L. et al. Peltier cooling in molecular junctions. *Nature Nanotechnology* **13**, 122-127 (2018).
93 Cui, L. et al. Quantized thermal transport in single-atom junctions. *Science* **355**, 1192-1195 (2017).
94 Mosso, N. et al. Heat transport through atomic contacts. *Nature Nanotechnology* **12**, 430-433 (2017).
95 Lumbroso, O. S. et al. Electronic noise due to temperature differences in atomic-scale junctions. *Nature* **562**, 240-244 (2018).
96 Cornia, A. & Seneor, P. The molecular way. *Nature Materials* **16**, 505 – 506 (2017).
97 Bogani, L. & Wernsdorfer, W. Molecular spintronics using single-molecule magnets. *Nature Materials* **7**, 179-186 (2008).
98 Lefter, C., Davesne, V., Salmon, L., Molnár, G., Demont, P., Rotaru, A. & Bousseksou, A. Charge Transport and Electrical Properties of Spin Crossover Materials: Towards Nanoelectronic and Spintronic Devices. *Magnetochemistry* **2**, 18 (2016).
99 Meded, V. et al. Electric control over the Fe(II) spin transition in a single molecule: Theory and experiment. *Phys. Rev. B* **83**, 245115 (2011).
100 Burzurí, E., García-Fuente, A., Garía-Suárez, V., Kuppusamy, S., Ruben, M., Ferrer, J. & van der Zant, H.S.J. Spin-state dependent conductance switching in single molecule-graphene junctions. *Nanoscale* **17**, 7905 – 7911 (2018).
101 Hayakawa, R. Large Magnetoresistance in Single-Radical Molecular Junctions. *Nano Lett.*, **16**, 4960-4967 (2016).
102 Heersche, H. B. et al. Electron Transport through Single Mn_{12} Molecular Magnets, *Phys. Rev. Lett.* **96**, 206801 (2006).
103 Burzurí, E., Zyazin, A.S., Cornia, A. & van der Zant, H.S.J. Direct observation of magnetic anisotropy in an individual Fe4 single-molecule magnet. *Phys. Rev. Lett.* **109** 147203 (2012).
104 Thiele, S. et al. Electrically driven nuclear spin resonance in single-molecule magnets. *Science* **344**, 1135-1138 (2014).
105 Vincent, R. et al. Electronic read-out of a single nuclear spin using a molecular spin transistor. *Nature* **488**, 357–360 (2012).
106 Godfrin, C. et al., Operating Quantum States in Single Magnetic Molecules: Implementation of Grover's Quantum Algorithm, *Phys. Rev. Lett.* **119**, 187702 (2017).
107 Park, J. et al. Coulomb blockade and the Kondo effect in single-atom transistors. *Nature* **417**, 722–725 (2002).
108 Liang, W. Kondo resonance in a single-molecule transistor. *Nature* **417**, 725–729 (2002).
109 Parks, J. et al. Tuning the Kondo Effect with a Mechanically Controllable Break Junction. *Physical Review Letters* **99**, 026601 (2007).
110 R. Temirov et al., Kondo effect by controlled cleavage of a single-molecule contact. *Nanotechnology*, **19**, 065401 (2018).
111 Rakhmilevitch, D., Tal, O. Vibration-mediated Kondo transport in molecular junctions: conductance evolution during mechanical stretching. *Beilstein J. Nanotechnol.* **6**, 2417–2422 (2015).

112 Frisenda, R., Gaudenzi, R., Franco, C., Mas-Torrent, M., Rovira, C., Veciana, J., Bromley, S.T., Burzurí, E. & van der Zant, H.S.J. Kondo effect in a neutral and stable all-organic single-molecule break junction. *Nano Letters* **15**, 3109-3114 (2015).
113 Appelt, W.H. et al., Predicting the conductance of strongly correlated molecules: the Kondo effect in perchlorotriphenylmethyl/Au junctions. *Nanoscale* **10**, 17738-17750 **(**2018).
114 J.J. Parks et al. Mechanical Control of Spin States in Spin-1 Molecules and the Underscreened Kondo Effect, *Science* **328**, 1370-1373 (2010).
115 Roch, N. et al. Observation of the underscreened Kondo effect in a molecular transistor, *Phys. Rev. Lett.* **103**, 197202 (2009).
116 Roch, N. et al. Quantum phase transition in a single-molecule quantum dot, *Nature* **453**, 633-637 (2008).
117 Requist, R. et al. Metallic, magnetic and molecular nanocontacts. *Nature Nanotechnology*, **11**, 499-508 (2016).
118 Scott, G. D. & Natelson, D. Kondo Resonances in Molecular Devices. *ACS Nano* **4**, 3560–3579 (2010).
119 Pietsch, T., Egle S., Keller M., Fridtjof-Pernau, H., Strigl, F. and Scheer, E.. Microwave-induced direct spin-flip transitions in mesoscopic Pd/Co hetereojunctions, *New Journal of Physics* **18**, 093045 (2016).
120 Vardimon, R., Matt, M., Nielaba, P., Cuevas, J.C. and Tal, O. Orbital origin of the electrical conduction in ferromagnetic atomic-size contacts: Insights from shot noise measurements and theoretical simulations, *Phys. Rev. B* **93**, 085439 (2016).
121 Rakhmilevitch, D., Sarkar, S., Bitton, O., Kronik, L. & Tal, O. Enhanced Magnetoresistance in Molecular Junctions by Geometrical Optimization of Spin-Selective Orbital Hybridization. *Nano Lett.*, **16**, 141 – 1745 (2016).
122 Pasupathy, A. N. et al. The Kondo Effect in the Presence of Ferromagnetism. *Science* **306**, 86 (2004).
123 Yoshida, K. et al. Gate tunable large negative Tunnel magnetoresistance in Ni-C_{60}-Ni single molecule transistors. *Nano Letters*, **13**, 481-485 (2013).
124 Scott, G. D. & Hu, T.C. Gate-controlled Kondo effect in a single-molecule transistor with elliptical ferromagnetic leads, *Phys. Rev. B*, **96**, 144416 (2017).
125 Brooke, R . J .et al. Single-Molecule Electrochemical Transistor Utilizing a Nickel-Pyridyl Spinterface. *Nano Letters* **15**, 275-280 (2015).
126 Naaman, R. & Waldeck, D. Spintronics and Chirality: Spin Selectivity in Electron Transport Through Chiral Molecules. *Annual Review of Physical Chemistry* **66**, 263-281 (2015).
127 Aragonès, A. *et al.* Measuring the Spin-Polarization Power of a Single Chiral Molecule. *Small* **13**, 1602519 (2016).
128 Franke, K.J., Schulze, G., & Pascual, J.I. Competition of superconducting phenomena and kondo screening at the nanoscale. *Science* **332**, 940-944 (2011).
129 Winkelmann, C. B. et al. Superconductivity in a single-C_{60} transistor, *Nature Physics* **5**, 876-879 (2009).
130 Island, J. O. et al. Proximity-Induced Shiba States in a Molecular Junction. *Phys. Rev. Lett.* **118**, 117001 (2017).
131 Brunner, J., González, M.T., Schönenberger, C. & Calame, M. Random telegraph signals in molecular junctions. *Journal of Physics: Condensed Matter* **26**, 474202 (2014).
132 Puczkarski, P. Wu, Q., Sadeghi, H., Hou, S., Karimi, A., Sheng, Y., Warner, J.H., Lambert, C.J., Briggs, G.A.D. & Mol, J.A. Low-Frequency Noise in Graphene Tunnel Junctions. *ACS Nano* **12**, 9451–9460 (2018).
133 Osorio, E.A., Ruben, M., Seldenthuis, J.S., Lehn, J.-M. & van der Zant, H.S.J. Conductance switching and vibrational fine structure of a [2x2]Co^{II}_4 grid-like single molecule contacted in a three-terminal configuration. *Small* **6,** 174-178 (2010).

134 Lemmer, M. et al. Unsupervised vector-based classification of single-molecule charge transport data. *Nature Communications* **7**, 12922 (2016).
135 Wu, B. H., Ivie, J. A., Johnson, T. K., and Monti Masel, O. L. A.. Uncovering hierarchical data structure in single molecule transport. *Journal of Chemical Physics* **146**, 092321 (2017).
136 Hamill, J.M., Zhao, X.T. Mészáros, G., Bryce, M.R. and Arenz, M. Fast Data Sorting with Modified Principal Component Analysis to Distinguish Unique Single Molecular Break Junction Trajectories. *Phys. Rev. Lett.* **120**, 016601 (2018).
137 Ward et al. Optical rectification and field enhancement in a plasmonic nanogap. *Nat. Nanotechnol.* **5**, 732-736 (2010).
138 Zolotavin, P., Evans, C., Natelson, D. Photothermoelectric Effects and Large Photovoltages in Plasmonic Au Nanowires with Nanogaps. *J. Phys. Chem. Lett.* **8**, 1739-1744 (2017).
139 Ittah, N., Selzer, Y. Electrical Detection of Surface Plasmon Polaritons by $1G_0$ Gold Quantum Point Contacts. *Nano Lett.* **11**, 529-534 (2011).
140 Benner, D. et al. Lateral and Temporal Dependence of the Transport through an Atomic Gold Contact under Light Irradiation: Signature of Propagating Surface Plasmon Polaritons. *Nano Lett.* **14**, 5218-5223 (2014).
141 Vadai, M. et al. Plasmon-Induced Conductance Enhancement in Single-Molecule Junctions. *J. Phys. Chem. Lett.* **4**, 2811-2816 (2013).
142 Fung, E-D. et al. Too Hot for Photon-Assisted Transport: Hot-Electrons Dominate Conductance Enhancement in Illuminated Single-Molecule Junctions. *Nano Lett.* **17**, 1255-1261 (2017).
143 Du, S., Yosiha, K., Zhang, Y., Hamada, I. & Hirakawa, K. Terahertz dynamics of electron-vibron coupling in single molecules with tunable electrostatic potential. Nature Photonics (2018), published on line.
144 Amdursky, N. et al. Electronic Transport via Proteins. *Advanced Materials* **26**, 7142-7161 (2014).
145 See for a recent review: Wang, K. DNA-Based Single-Molecule Electronics: From Concept to Function. *J. Funct. Biomater.* **9**, 8 (2018).
146 Li, W.-Q., et al. Detecting electron transport of amino acids by using conductance measurement, *Sensors* **17** 811 (2017).
147 Xiao, X., Xu, B. & Tao, N. Conductance Titration of Single-Peptide Molecules. *J. Am. Chem. Soc.* **126** 5370-5371 (2004).
148 Brisendine, J.M. et al. Probing charge transport through peptide bonds. *J. Phys. Chem. Lett.* **9**, 763–767 (2018).
149 Artés, J.M. et al. Nanoscale charge transfer in redox proteins and DNA: Towards biomolecular electronics, *Electrochimica Acta* **140** 83–95 (2014).
150 Galperin, M., Ratner, M.A. & Nitzan, A. Molecular transport junctions: vibrational effects. *J. Phys.: Condens. Matter* **19** (2007) 103201.
151 Park, H. et al. Nanomechanical oscillations in a single-C60 transistor. *Nature* **407**, 57–60 (2000).
152 Koch, J. Theory of the Franck-Condon blockade regime. Phys. Rev. B 74, 205438.
153 Burzurí, E. et al. Franck–Condon Blockade in a Single-Molecule Transistor. *Nano Letters* **14**, 3191–3196 (2014).
154 Yu, L. H. et al. Inelastic Electron Tunneling via Molecular Vibrations in Single-Molecule Transistors. *Phys. Rev. Lett.* **93**, 266802 (2004).
155 Isshiki, Y., Matsuzawa, Y., Fujii, S. & Kiguchi, M. Investigation on Single-Molecule Junctions Based on Current–Voltage Characteristics. *Micromachines* **9**, 67 (2018).
156 Seldenthuis, et al. Vibrational Excitations in Single-Molecule Junctions. *Handbook of Single-Molecule Electronics* 1st edition, 155-204 (2015).

157 Wang, Y.-H. et al. Conductance measurement of carboxylic acids binding to palladium nanoclusters by electrochemical jump-to-contact STM break junction. *Electrochim. Acta* **123**, 205-210 (2014).
158 Prins, F. et al. Platinum-nanogaps for single-molecule electronics: room-temperature stability. *Phys. Chem. Chem. Phys.* **13**, 14297-14301 (2011).
159 Guédon, C. M. et al. Observation of quantum interference in molecular charge transport. *Nature Nanotechnology* **7**, 305-309 (2012).